THE DESIGN OF A HIGH RESOLUTION ELECTRON BEAM MACHINE

by

Norman Matheson Lindsay, B.Sc.

Thesis presented for the degree of Doctor of Philosophy of the University of Edinburgh in the Faculty of Science.

September, 1969.

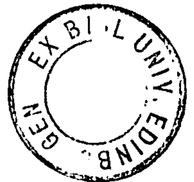

ABSTRACT

A review of electron beam processes for the manufacture of micro-circuit devices is followed by examples of current design in electron beam machine (EBM) systems. The main features of the system under present study are then explained. The important electron-optical and general system parameters of the EBM are enumerated and discussed.

The performance of the electron gun and deflection systems are of particular importance in the EBM application. A field emission gun would contribute well to the performance of the EBM, but this introduces problems since stable field emission only occurs in an ultra high vacuum environment.

An extension of conventional digital-to-analog converter designs has yielded a wide range precision digital-to-analog function generator circuit, which is specially suited to EBM requirements. Special attention has also been paid to all other electronic instrumentation within the system, with a view to meeting particular function and performance.

The final chapter summarises the work, and indicates the direction of future development.

CONTENTS

CHAPTER 1	INTRODUCTION	
1.1	Modern techniques	1
1.2	Intercol	4
1.3	Deflection signal generators	7
1.4	The experimental UHV system	11
CHAPTER 2	PROPERTIES OF ELECTRON-OPTICAL SYSTEMS	
2.1	Electron motion in electric and magnetic fields	15
2.2	Magnetic lenses	16
2.3	Diffraction aberration	18
2.4	Spherical aberration	20
2.5	Chromatic aberration	24
2.6	Source brightness	25
2.7	Deflection aberrations	27
2.8	Asymmetry of the fields	32
2.9	Parasitic fields	34
2.10	Mechanical instability	35
2.11	The interaction at the workpiece surface	36
CHAPTER 3	THE ELECTRON SOURCE	
3.1	Electron emission	39
3.2	Thermionic versus field emission	42

CHAPTER 3 (contd.)

3.3	Fabricating the tip	47
3.4	Field emission experiments	53
3.5	Three electrode controller	59
CHAPTER 4	FORMING THE PROBE	
4.1	System N° 1	66
4.2	System N° 2	76
CHAPTER 5	THE BEAM DEFLECTION SYSTEM	
5.1	D-to-A generator	81
5.2	Pantograph controller	89
5.3	Deflection coil design	94
CHAPTER 6	REVIEW	100

CHAPTER 1

INTRODUCTION

There are numerous systems now being used to fabricate microelectronic devices by directing the energy of a focussed electron beam to shape the device. Such a system is generally labeled an "electron beam machine" or EBM. This use for electron beams developed from the high powered electron beam welders which make precision welds and cuts in a variety of materials, including such intractable materials as aluminium oxide and tungsten, by melting or vapourising material at the focus of the beam. For microelectronic purposes, using relatively low energy electrons and smaller beam currents, the same technique can be used to vapourise micron dimension channels in thin films[1].

1.1 MODERN TECHNIQUES

In recent years "electron-optical" processes, which utilise properties other than the thermal energy of an electron beam, have been tried with considerable success. These processes involve surface chemical reactions and can be divided into two main categories, polymerisation processes and activated chemical deposition processes. In the first case the electron beam irradiates the target surface in the presence of an organic compound to produce a polymer film. The organic

compound may be introduced into the system in the vapour phase or as a solid such as a photoresist coating. The second case is very interesting, as both metallic and dielectric films can be produced. The film is formed as a result of direct decomposition by electron beam bombardment of a suitable chemical compound already present on the target surface. An organo-metallic compound is usually used to produce metallic films, and insulating films have been produced from tetraethylorthosylicate.*

The above methods are not at present widely used in the commercial manufacture of microcircuits, but they are potentially capable of reducing the dimensions of present day microcircuits by at least one order of magnitude. Using electron-optical techniques, Thornley and Hatzakis(2) have already demonstrated the viability of producing high speed planar silicon transistors with 1μ detail, and this is to be compared with detail of about 2.5μ using conventional techniques. Chang and Nixon(3) have experimented with the electron beam polmerization of silicone oil vapour and can now produce circuit detail of 500 Å. They have also considered the theoretical factors which limit the ultimate resolution obtainable with this technique.

Any EBM can be modified to operate as a scanning electron microscope, and indeed the converse of this is true. In the experiments

---

*A summary of work by various authors on electron-optical processes appears in reference (3).

referred to above, Chang and Nixon operate a standard scanning electron microscope system as an EBM. In its simplest form a scanning electron microscope requires a very low current electron probe to scan the surface of the specimen under examination, and a method for detecting and amplifying the secondary electron emission from the specimen[4]. This amplified signal then modulates a CRT beam which is scanned in synchronism with the electron probe, forming a magnified image of the specimen surface. Thus, in the EBM we have a machine that can extend the limits of circuit miniturization, and affords a means for examining and testing the circuit as it is being machined.

There seems enough evidence to predict that the EBM will grow in importance. This thesis presents a report on the development of a prototype high resolution EBM system, where an attempt has been made to obtain a high performance system which is at the same time easy to operate and mechanically simple. The work started using an EBM system already operating in our laboratory as a testing ground for new ideas. However it was decided at an early stage of the project that a completely new prototype was required as major changes in the design were to be introduced. This introductory chapter will follow with a description of the original EBM which should give a clear idea of the type ofsystem typical of the great majority being used today, and later describe the main points of difference in the new experimental system.

1.2 - INTERCOL

Figure 1.1 shows a diagram of "Intercol", which is an EBM system developed by Electron Physical Instruments Ltd.[5] The basic components are an electron gun and lens system capable of providing a focussed spot of down to 1μ diameter, which can be deflected without serious defocussing over a millimetre square.

The gun assembly which is all at the EHT potential, consists of a hairpin type tungsten filament and re-entrant control grid. The EHT, bias, and filament supplies are connected to the gun by means of a plug and socket. Lateral filament adjustment is made by four adjusting screws situated in the main gun body, and provision is also made for vertical adjustment of the filament. These adjustments locate the filament centrally relative to the control grid, and vary the filament to grid spacing to obtain optimum performance. The filament has a life of about 30 hours, and during operation slight movement of the filament occurs requiring periodic readjustment.

The lens body housing the energising coil is identical for both lenses, the pole pieces being attached separately and allowing flexibility in the focal properties of the lenses. The position of the pole pieces are asymmetric within the bores, and as the lenses can be inverted this permits a choice of position for the focussing field along the beam axis. Provision is made for adjusting the

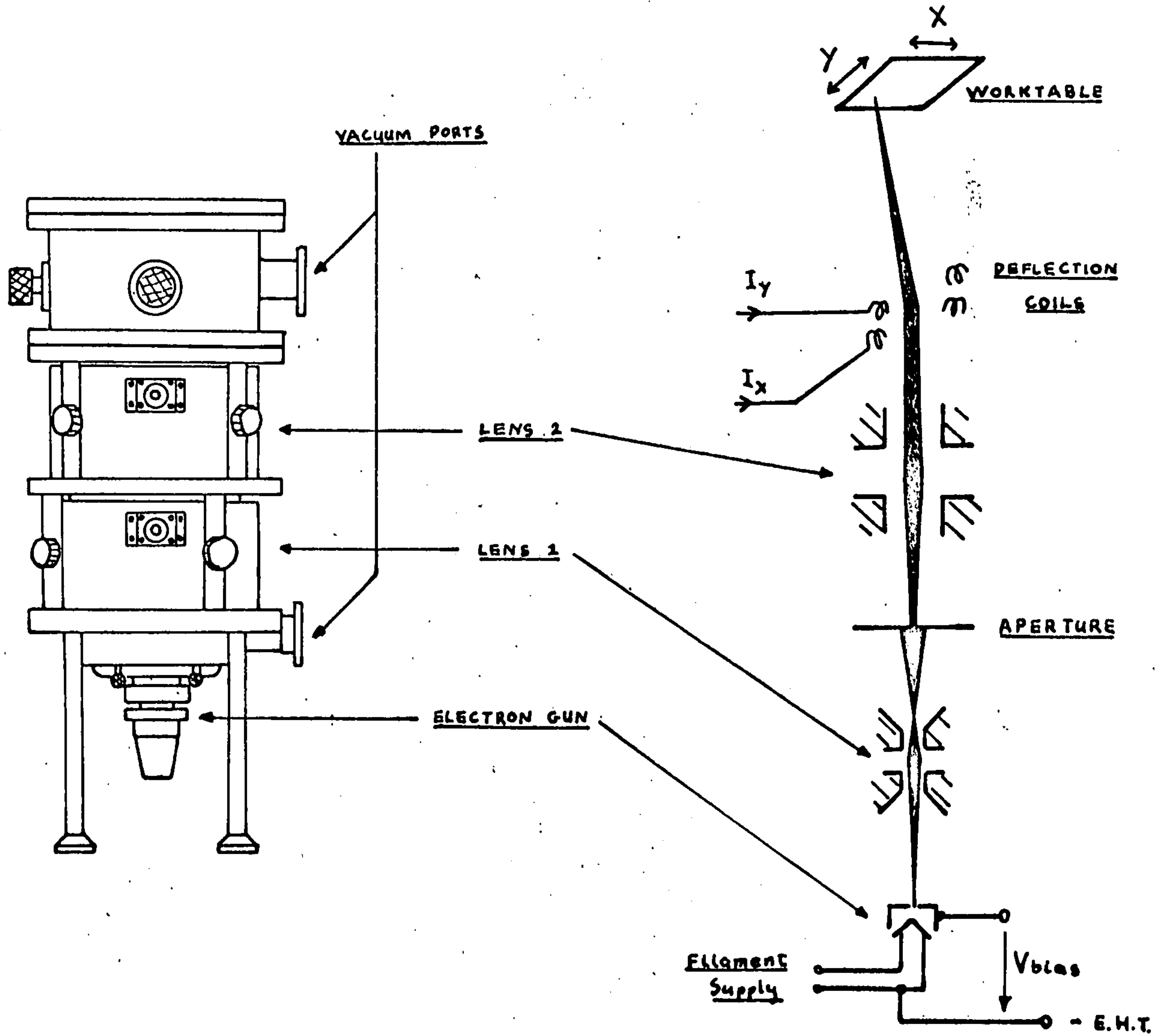

Figure 1.1 INTERCOL

position of each lens in the X-Y plane (i.e. the plane perpendicular to the beam axis). An aperture changer is fitted to both lenses.

The work chamber is fairly large, being 8" in diameter by 5" deep and fitted with a 3" glass viewing port at the top. A co-ordinate stage allows the workpiece (e.g. thin film substrate) to be moved within the vacuum chamber. The stage covers an effective area of 2" x 2" and has direct mechanical linkage through the vacuum envelope via special seals. Also provided are a vacuum port and a termination port which permit electrical connections to be made to components within the vacuum envelope. Between the final lens and the work chamber a small space allows room for the X and Y deflection coils. In the bore of the lens a "blanking" coil has been fitted, which deflects the beam across an aperture and effectively cuts off the beam.

Essential ancilliary equipment are the high vacuum system and the electronic power supplies for the electron gun and the lenses. The high vacuum system has been designed to give a pump-down time from atmosphere to 10^{-5} Torr of about ten minutes, using a rotary pump and a water cooled oil diffusion pump. The EHT will deliver from 5 to 30 kV at up to 2mA, but the best results for high resolution have been obtained with final beam currents of about 0·1 to 1μA at energies of around 10kV.

1.3 DEFLECTION SIGNAL GENERATORS

With any EBM it is necessary to have some source for the signals to the X and Y coils controlling the beam position on the workpiece. This source or generator must provide a means for translating the drawing board design into the proper electrical signals. Figure 1.2 outlines three systems commonly adopted to do this job, each method having its own special advantages.

The basic idea of the flying-spot scanner has been borrowed from television engineering. A conventional black and white slide of the required pattern is illuminated by a cathode ray tube spot, scanned across its area. On the other side of the film transmitted light is picked up by a photocell, and the signal produced modulates the beam blanking coil, while at the same time the machining electron beam is being scanned in synchronism with the CRT beam. Thus a pattern can be transferred from a drawing to film, providing a convenient program to be run automatically and later stored for future use. The main drawback with this method is that it does not trace out the pattern continuously, which results in some loss of resolution. The system is nevertheless very fast and reasonably inexpensive.

The electric pantograph is cheap and versatile. Figure 1.2 (b) shows a very crude form of electric pantograph for EBM control.

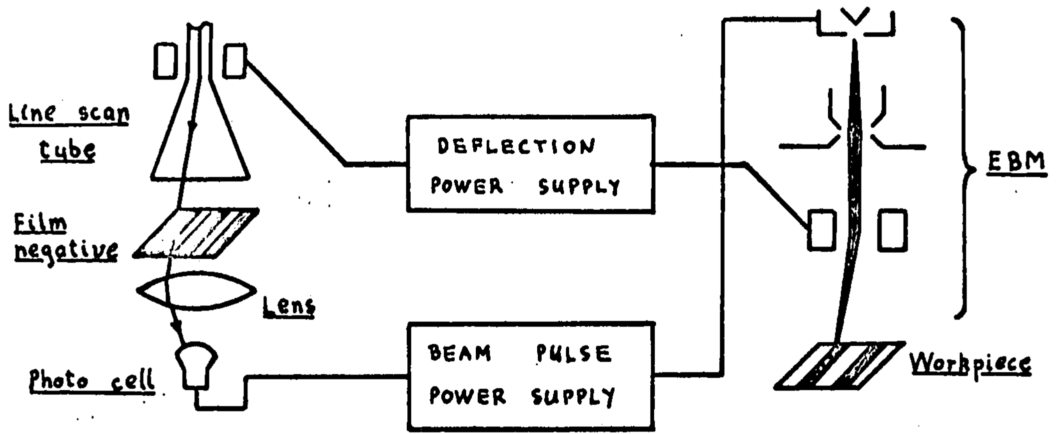

(a) Flying-spot scanner

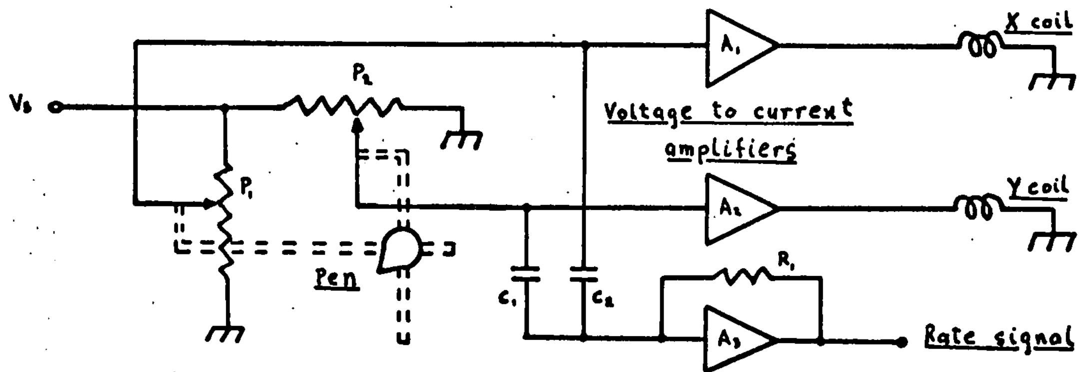

(b) Pantograph

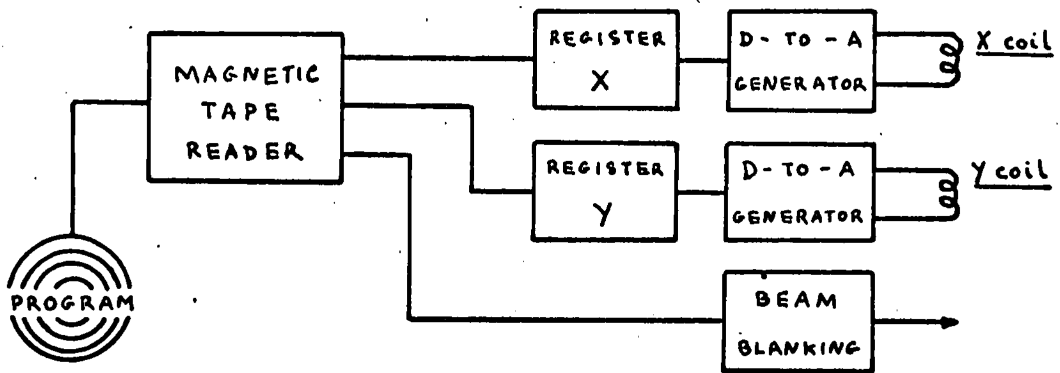

(c) Digital control

Figure 1.2 Deflection control systems

The pen is free to move and is mechanically linked to the potentiometers P_1 and P_2 such that voltages proportional to the X - Y position of the pen are fed to the differential amplifiers. This technique is suitable for tracing patterns of continous lines, especially in cases where preliminary tests are being carried out on prototypes, since although a rather slow method, a designer can sit down and directly transcribe his ideas to the EBM. For satisfactory results a more sophisticated version is desirable, with pneumatic damping of the pen to eliminate hand shake, and possibly control of the pen speed by servomechanisms to achieve very uniform beam traverse velocity. An alternative method would be to modulate the beam current by signals proportional to the rate of movement of the pen. This would ensure delivery of constant charge per unit area of workpiece, and for the special case of the pen at rest, it would blank the beam. As shown on the diagram, signals proportional to rate of pen movement are derived from C_1 and C_2. It is felt that some form of electric pantograph generator should eventually be included in our EBM set up, as it would provide a flexible alternative signal source.

The most sophisticated method of control is by digital computer (figure 1.2(c)). This can either be done with an on-line computer, or by playing a pre-recorded program through a digital tape reader. Also required is a computer-EBM interface. This is usually composed of two registers for the X and Y co-ordinates, which feed into

digital-to-analog-current converters controlling the currents in the X-Y coils, and also a gate controlling the beam blanking unit. This basic system can be elaborated on to a great extent by for example, adding computer control of the beam current, voltage, and spot size, plus any other variable it is felt necessary to control. Futher, after a machining operation the computer can switch the EBM to a scanning electron microscope mode and analyse the results fed back to it. The workpiece would then be passed, or rejected, or further machining to correct errors would be computed and carried out.

The control unit for the Intercol in our laboratory is a digital version, with an extremely simple but readily programmed computer. Two 10-bit digital-to-analog-current converters generate the X and Y currents, and the number of increments required in the X or Y direction is set up manually on a control switch board. (Thus a fair amount of human computation is required). An "operate" switch, switches on the electron beam, and the correct number of pulses are generated at a pre-determined rate and counted on the X or Y register. The beam is then switched off. This method, like the electric pantograph, is easily programmed but slow and mainly suitable for prototype circuits, though it is much more accurate than the pantograph. Arrangements are now being made to have magnetic tape input, and it is hoped at a later date to operate "on-line" the departmental PDP8 computer.

1.4 THE EXPERIMENTAL UHV SYSTEM

Figure 1.3 is a sketch of the new EBM in its present experimental form. A special feature of this system is that it operates at ultra high vacuum (UHV), so that in this case the vacuum system and electron beam column are made of stainless steel. The two main disadvantages of a UHV system are that it is generally more expensive and it is very difficult to achieve a fast pump-down. To alleviate these drawbacks, the volume and the mechanical complexity of the system has been reduced to a minimum, thereby allowing the total component cost to compare favourably with that of the Intercol system. Unfortunately the pump-down time needs to be much improved, but meanwhile the system is being used to assess the undoubted advantages afforded by UHV. The principal reason for using UHV was to allow the operation of a field emitter source. This type of emitter or cathode gives the best performance for EBM purposes, but should be operated at pressures of the order of 10^{-9}Torr or better, since at higher pressures the cathode rapidly becomes contaminated and unusable. A second important advantage is that the UHV pumps are also ultra clean, so we are provided with the best possible environment for accurate and reliable operation.

The field emitter forms part of a pre-aligned three-electrode electron gun, and should remain permanently aligned since the field emitter, operating at ambient temperature, is mechanically very stable.

This eliminates the need for a high vacuum mechanical feedthrough for cathode adjustment.

The single lens is an air cored solenoid wound outside the vacuum envelope. The deflection coils are also wound outside the column. The column comprises a single, standard, stainless steel unit. There is no co-ordinate stage to allow mechanical displacement of the workpiece, but this lack is made up for by designing the deflection system to have a very wide dynamic range, and by providing for dynamic focussing of the solenoid lens, so that the beam can be scanned over a relatively large area without increasing the spot size.

The main design concepts of the prototype have been summarised. It now remains to discuss the design in detail.

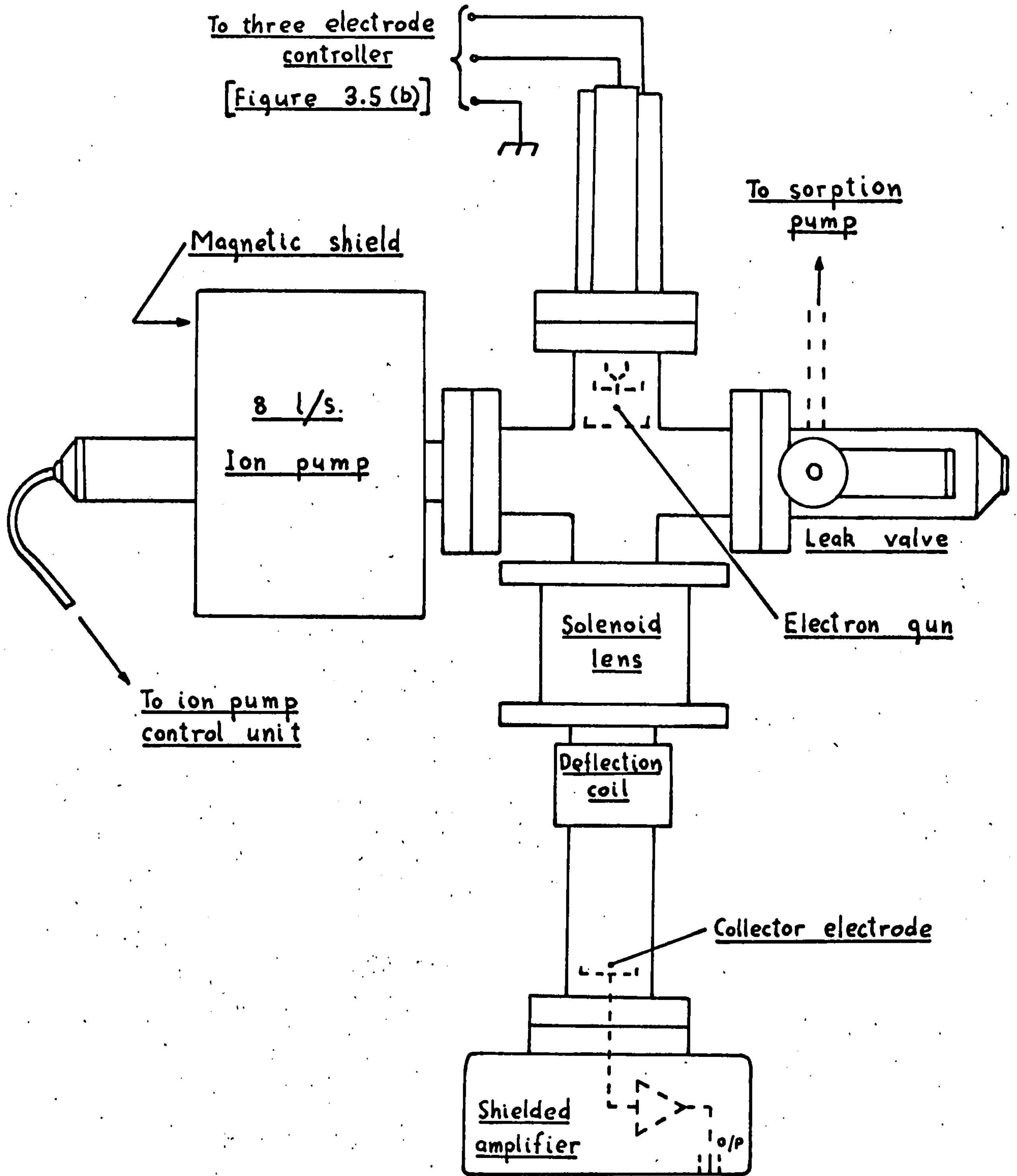

Figure 1.3 UHV system

Figure 1.4 Experimental EBM

CHAPTER 2

PROPERTIES OF ELECTRON-OPTICAL SYSTEMS

In this chapter we will look at the problem of forming and deflecting a finely focussed electron beam. The main topics discussed will be the aberrations inherent in the electron-optical components, or introduced by the associated electronic instrumentation, or by other extraneous causes.

2.1 ELECTRON MOTION IN ELECTRIC AND MAGNETIC FIELDS

We are here only interested in low energy electrons (e.g. with energies less than 20keV) so electron motion will be non-relativistic. Let us recall two of the basic equations of motion for an electron, derived from the Lorentz equation for an electron.

$$ma = - e(E + v \wedge B) \tag{2.1}$$

where a = electron acceleration $(a = \dot{v} = \ddot{s})$
v = electron velocity $(v = \dot{s})$
(s = electron path)
e = electron charge
m = electron rest mass
E = electric field strength (volts/metre)
B = magnetic field (tesla)
(V = accelerating potential in volts)

Multiplying both sides of (2.1) by v.dt and then integrating we have

$$m\int \dot{v}.v.dt = -e\int E.ds$$

$$\tfrac{1}{2}mv^2 = eV + \text{constant} \qquad (2.2)$$

$$(\text{since } v_\wedge B.v = 0)$$

Assuming the electron velocity is zero when V = 0 the velocity of the electron is given by

$$v = (2e/m)^{\frac{1}{2}}.V^{\frac{1}{2}} \qquad (2.3)$$

For a purely magnetic field the Lorentz force is perpendicular to v and B, and if B is constant then the electron path is in general a spiral with circular radius R. The $ev_\wedge B$ force is balanced by a centrifugal force, mv^2/R, so we can equate these terms and arrive at

$$1/R = (e/2mV)^{\frac{1}{2}}.B \qquad (2.4)$$

2.2 MAGNETIC LENSES

A general rule which appears in nearly all textbooks on electron-optics, is that magnetic lenses and magnetic deflection systems almost invariably exhibit less aberration than do electrostatic lenses and deflectors, and so for our purposes magnetic systems are preferred.

We shall consider a simple case of a magnetic lens field. A basic

equation we will require is the paraxial ray equation for axially symmetrical magnetic fields*.

$$r'' = \frac{-e}{8mV} B(z)^2 . r \qquad (2.5)$$

where r = electron radius about the z-axis
$r' = dr/dz$
$r'' = d^2r/dz^2$
$B(z)$ = z component of magnetic field

Figure 2.1 shows a simple lens with circular symmetry about the z-axis. The real lens is replaced by an ideal lens of "equivalent length" L, such that $B(z) = B_0$ = constant between $z = 0$ and $z = L$, and the field is zero elsewhere. L is defined by

$$L = B_0^{-2} \int_{-\infty}^{\infty} B(z)^2 . dz \qquad (2.6)$$

Although this is a fictitious approximation, it still yields a fairly accurate result for the convergence of the lens. For an electron path defined by $r = r_0$ and $r' = 0$ at $z = 0$, an appropriate solution for equation (2.5) inside the field is

---

*For a derivation see for example reference (6).

$$r = r_0 \cos(e/8mV)^{\frac{1}{2}} B_0 z$$
$$r' = - r_0 (e/8mV)^{\frac{1}{2}} B_0 \sin(e/8mV)^{\frac{1}{2}} B_0 z \qquad (2.7)$$

For cases where the real focus lies outside the lens the focal length f is given by $- r_0/r_L'$ where r_L' is the slope at $z = L$, and thus

$$f = 1/(k \sin kL) \qquad (2.8)$$

where $k = (e/8mV)^{\frac{1}{2}} B_0$

For weak lenses where $f \gg L$ we have $\sin(kL) \doteq kL$ and

$$f = 1/(k^2 L) \qquad (2.9)$$

In the majority of magnetic lenses the axial field B(z) is bell-shaped so a more accurate analysis can be made by finding a simple mathematical model to represent the bell-shaped fields. The classical Glaser model[7] can describe to within a few percent the properties of magnetic lenses with a wide variety of pole-pieces.

Finally the paraxial equation may be solved for any distribution using step-by-step methods. Here the field distribution of the lens may be found by direct measurement[8] or by simulating the field on a resistance network analog.[9]

2.3 DIFFRACTION ABERRATION

In light optics it is theoretically quite possible to construct a

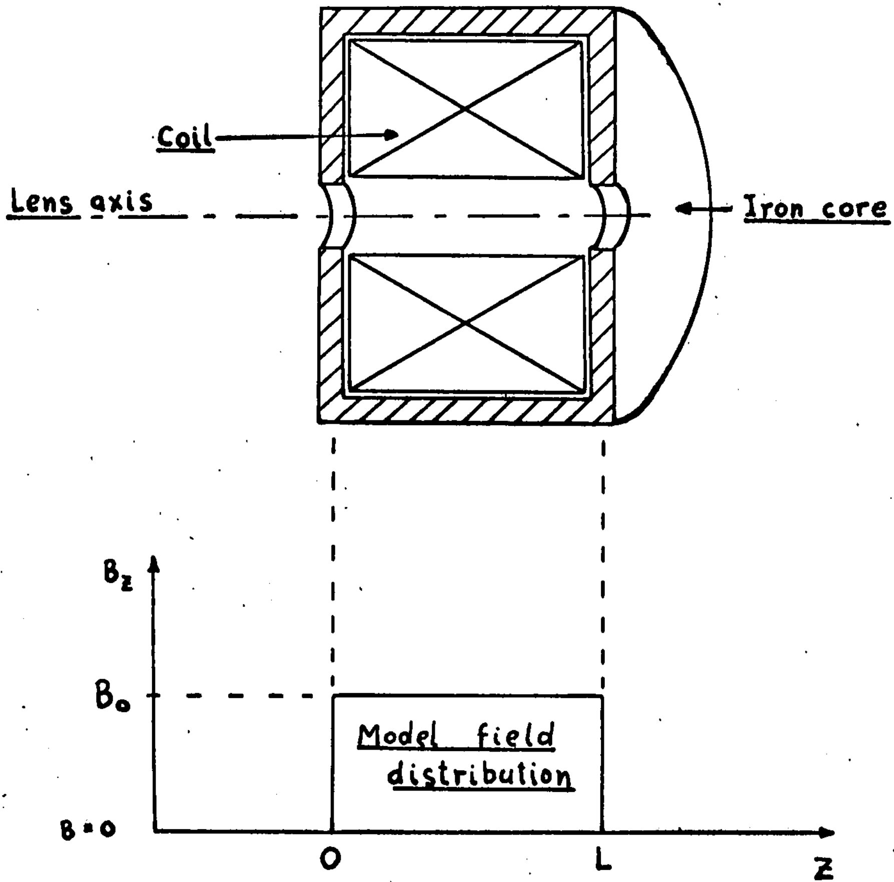

Figure 2.1 Magnetic Lens

lens system with no significant aberrations. The final resolving power is determined by diffraction, which is a characteristic of the radiation used in the microscope. The resolving power is fixed by λ the wavelength of the radiation, by α the angular aperture of the instrument, and by n the refractive index of the medium which surrounds the object. In practice a resolution of about $\frac{1}{2}\lambda$ is feasible if one uses a wide aperture objective lens which has been carefully corrected for aberrations.

For ultra-violet radiation λ is about 0.25μ, while the mean wavelength for visible light is 0.6μ. This is to be compared with the very small wavelength associated with a high energy electron. Even for a 10keV electron we have λ approximately equal to 0.12Å, and for electron-optics a first order approximation for the resolving power is given by

$$r_d = 0.6\lambda/\alpha \qquad (2.10)$$

where r_d is the radius of the focussed spot. For this equation to be accurate the angular aperture α must be restricted to small values.

2.4 SPHERICAL ABBERATION

It is unfortunately impossible to realise an electron lens which will work with the large apertures possible in glass optics. We now come up against "spherical aberration" or as it is sometimes called

"the aperture defect", and due to this defect inherent in all electron lenses, we find that to obtain optimum resolution the electrons must be confined by very small apertures.

The paraxial ray equation (2.5) is essentially a first order approximation. The first order theory of optics is often referred to as "Gaussian optics" after its originator, and equation (2.5) is otherwise known as the Gaussian equation. By taking into account third order terms neglected in the Gaussian equation we have the "third order theory", which is more applicable to situations where there are finite apertures.

Even with an idealised field as in figure 2.1 , it is found that the lens converges marginal rays more rapidly than rays close to the axis (see figure 2.2). Thus the image in the Gaussian image plane of a point object on the axis, is spread out over a spot of radius r_s proportional to α^3. Explicit formulae for spherical aberration can be derived for the lens models mentioned in section 2.2, by using the third order theory.

The radius of the aberration disc in the Gaussian image plane is given by

$$r_s = C_s\alpha^3 \qquad (2.11)$$

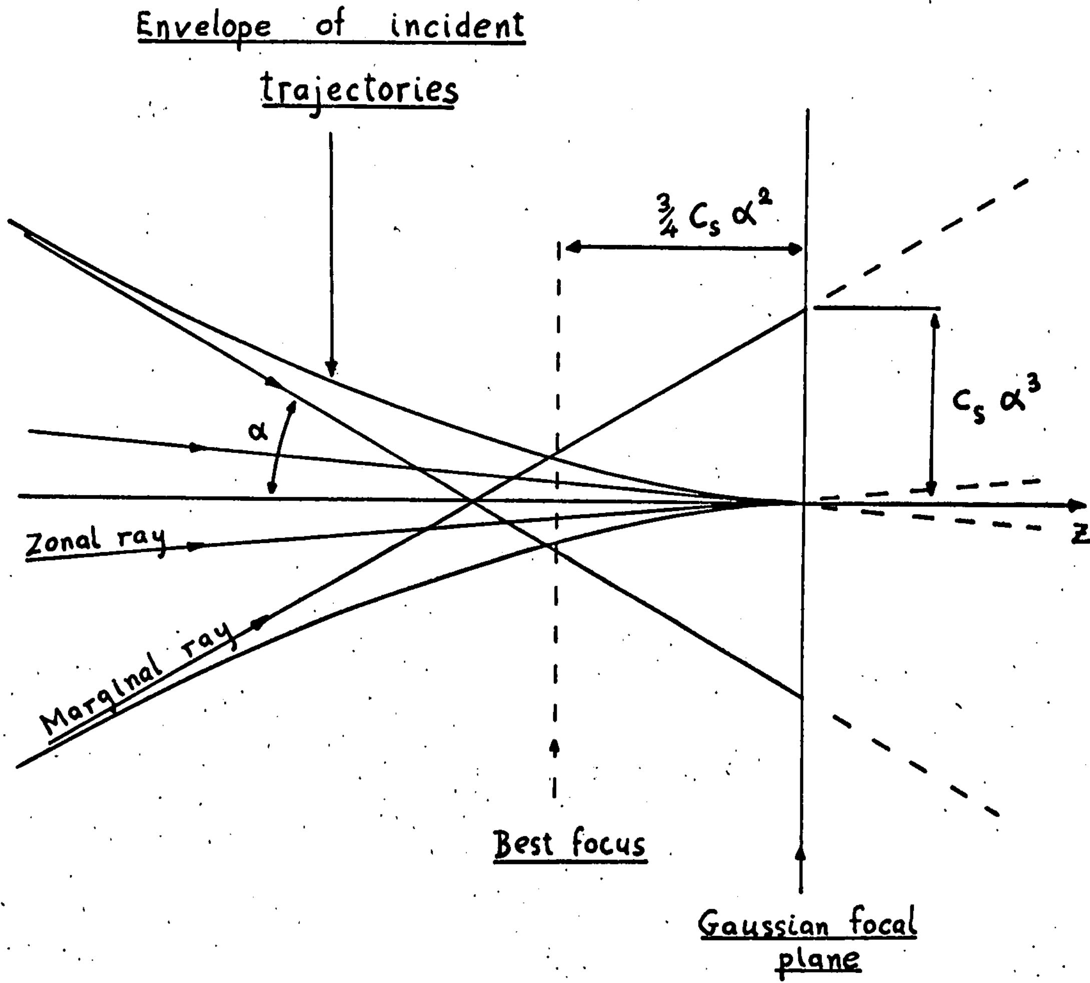

Figure 2.2 Spherical aberration

while the minimum beam cross-section is $\frac{1}{4}r_s$ and is located in a plane situated at a distance Δf from the Gaussian focal plane, where

$$\Delta f = -\tfrac{3}{4}C_s\alpha^2 \qquad (2.12)$$

Here C_s is the spherical aberration constant or cofficient which has the dimensions of length, and is related to the field distribution and the convergence of a given lens.

C_s is affected by many different parameters. In general the aberration diminishes rapidly if very intense fields are used, but there is an upper limit for B_0 of about 2.6 tesla, beyond which the saturation flux density of the best pole-piece material is reached. The pole-piece dimensions are also critical, and Liebmann[10] finds a practical optimum for the ratio of pole-piece spacing to bore diameter S/D , occurs in the zone $1 < S/D < 2$.

All practical lenses in EBM or similar electron-optical systems suffer from spherical aberration*, so to reduce this error we must make the apertures vanishingly small, but then we would introduce the diffraction error defined by equation (2.10).

---

*Strictly speaking, systems of lenses which can compensate spherical aberration have been proposed, but in general the accompanying complications prohibit their use in practical systems.

2.5 CHROMATIC ABERRATION

We have shown that the convergence of a magnetic lens (equation (2.9)) depends on the function V/B^2, where V is the accelerating potential and B is the axial magnetic field. By differentiating equation (2.9) with respect to V and B and then rationalising the expressions, we can define the incremental variations in the focal length arising from small fluctuations in V and B by

$$\Delta f/f = \Delta V/V \qquad (2.13)$$

$$\text{and} \quad \Delta f/f = -\, 2\Delta B/B \qquad (2.14)$$

The analogous situation in light optics is the variation with colour of the refractive index of a glass lens, and this aberration in the electron-optical situation is called "chromatic aberration". The fluctuations will manifest themselves by enlarging the focus on the Gaussian image plane by an amount proportional to $\alpha.\Delta f$. The constant of proportionality C_c , characterises the shape and disposition of the lens and is sometimes called the "form factor". Although C_c may be less than unity for a magnetic lens[10], it cannot be reduced to zero by manipulating the field distribution, but the ratios $\Delta V/V$ and $\Delta B/B$ are more amenable to control.

Chromatic aberrations arising from fluctuations in the EHT and lens supplies presents no serious difficulty. Using components

currently available, one can readily obtain short term stability (e.g. for one hour) of better than 1 part in 10^5 for a 20kV supply and for the lens supplies. It is also a simple matter to reduce supply ripple to below 1 part in 10^6.

The velocity dispersion of the electrons is the most serious and less avoidable contribution to the chromatic aberration. For a tungsten filament source operating at a temperature of T°K, the electrons have a distribution of initial velocities associated with their thermal energy. The operating temperature is typically 2700°K, and the majority of the electrons are then emitted with velocities between zero and one volt, and about one half of these have a velocity below 0.45 volts, so that ΔV is approximately 0.45 [11]. ("Velocity" is here understood as the equivalent accelerating voltage). For systems using very large accelerating potentials the error introduced by a 0.45 volt spread is relatively insignificant, but as we shall see, the requirements for optimum resolution in the EBM process impose an upper limit for the beam potential.

2.6 SOURCE BRIGHTNESS

A fundamental parameter of the focussed electron beam is the brightness at any crossover. This relates current density and convergence at the crossover, and is defined as the current per

unit area per unit solid angle of convergence.

In 1937 Langmuir[12] published his formula relating the intensity of the electron source and the focussed spot or crossover.

$$j_s/j_c = (11{,}600V/T)\alpha_s^2 \qquad (2.15)$$

where j_s = current density at spot
j_c = current density at cathode
V = accelerating potential (volts)
α_s = angular semi-aperture at the spot (radians)
T = absolute temperature of cathode (°K)

First, this implies that the crossover intensity is directly dependent on the current density and temperature of the source. Secondly, in a region of uniform potential the best theoretical brightness at the crossover(s) is invariable, and in practice this is reduced by lens aberrations. The effect of temperature on the brightness follows from the discussion in the previous section.

Equation (2.15) applies to thermionic emitters, but is not applicable to field emitters where the mechanism of electron emission is different (see chapter 3, section 3.1). A field emitter may operate near absolute zero but still has a significant distribution of initial electron energies[13]. The case of the field emitter has been analysed by Everhart[14], and he shows that the brightness of this source is several orders of magnitude

greater than a thermionic emitter. This is due to its higher emission density and also the greater coherence of the electrons.

2.7 DEFLECTION ABERRATIONS

The aberrations introduced by the deflecting fields are an important consideration, especially where a large dynamic range is required. (Dynamic range is here defined by the ratio of maximum "push-pull" deflection distance to diameter of the focussed spot).

For a mono-energetic electron the curvature of its trajectory is given by equation (2.4). Figure 2.3(a) illustrates the case of a conical beam originally converging on the axis at $Z = Z_f$. For convenience rectangular co-ordinates are adopted, and the deflecting field is assumed to be uniform and perpendicular to the page. For any electron in the beam the incremental change in direction $\Delta\theta$ is equal to $\Delta s/R$, where Δs is the incremental path length projected on the X = 0 plane.

An electron emerges from the field with an angle

$$\theta_1 = (e/2mV)^{\frac{1}{2}}.B.s_1 \qquad (2.16)$$

where $$s_1 = \sum_{Z=0}^{Z=1} \Delta s$$

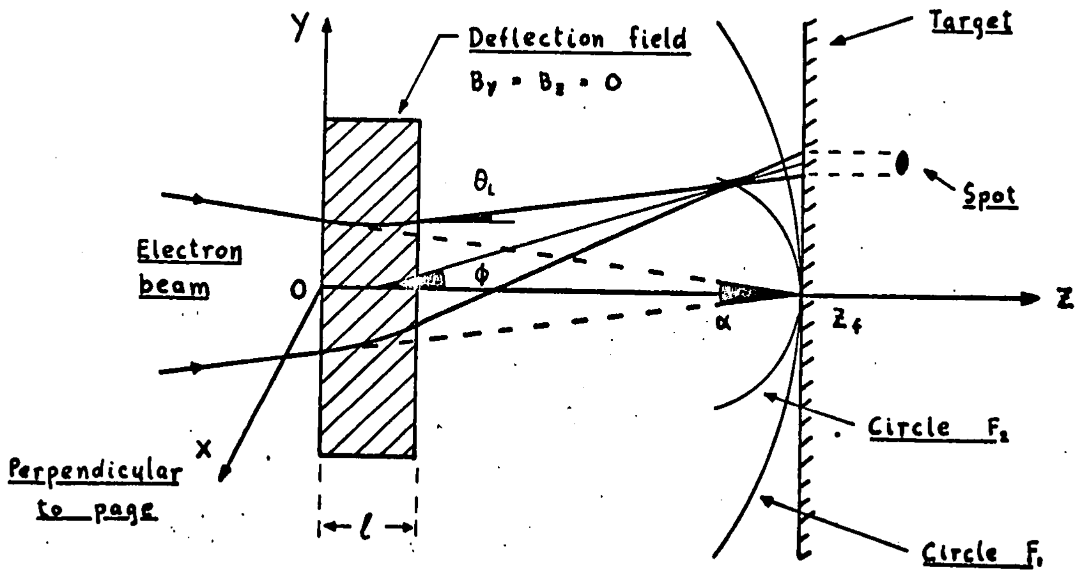

(a) Astigmatic over-focussing

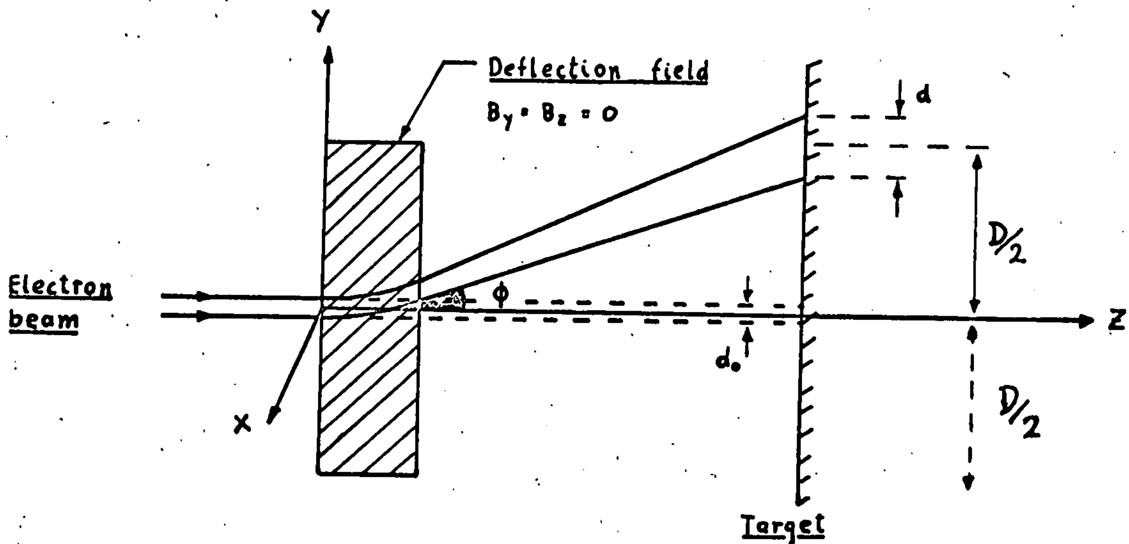

(b) Chromatic defocussing

Figure 2.3 Deflection aberrations

Now electrons originally in the $Y = 0$ plane will focus where their projected path length s_f is equal to Z_f . If the working distance Z_f is much larger than the width of the field 1, the locus of $s_f(\phi)$ for small deflection angles ϕ is a circle F_1 as shown. However in the $X = 0$ plane, electrons on the inside of the curve are under-deflected and those on the outside are over-deflected for correct focussing on the circle F_1 . In this plane the circle of focal points F_2 has a shorter radius, and this radius is a function of α the beam convergence angle, as well as ϕ . The effect on the image plane is an enlarged spot of elliptical shape, or in other words the spot is over-focussed and astigmatic.

A first order correction of this aberration is to use "dynamic focussing" and increase the focal length as the beam is deflected, so that the disc of least confusion (between F_1 and F_2) is projected on the $Z = Z_f$ plane.

If the field is altered so that B_x has a small component which increases with Y (a "pin-cushion" field), we can visualise from figure 2.3(a) that the over-focussing in the $X = 0$ plane is diminished or even reversed. Wang(15) has shown that for deflection in one plane only the field distribution can be optimised to eliminate astigmatism. However for the case of two separate field excitations in the X and Y directions, it is more difficult to obtain a non-astigmatic field(16). Schlesinger and Wagner

have used dynamic focussing and in addition dynamic control of astigmatism, with greatly improved resolution for deflection in two dimensions[17].

With deflecting fields a special case of chromatic aberration arises. In figure 2.3(b) the deflecting field is as before, but the beam is considered to be a narrow parallel pencil of diameter d_o. Such a beam will experience neither over-focussing nor astigmatism, since the trajectories through the field are all parallel. For the situation where the beam voltage V cannot be regarded as constant, an electron emerges with an angle proportional to $V^{-\frac{1}{2}}$.

$$\text{i.e.} \qquad \phi = K.V^{-\frac{1}{2}} \tag{2.17}$$

$$\text{and} \quad \Delta\phi/\phi = -\tfrac{1}{2}\Delta V/V \tag{2.18}$$

where ΔV is the energy spread in the beam. Due to ΔV the spot is elongated in the direction of the deflection, effectively increasing d (the diameter of the spot).

$$d = d_0 + \Delta\phi(\tfrac{1}{2}D/\sin\phi) \tag{2.19}$$

For small angles $\sin\phi \doteqdot \phi$, so combining equations (2.18) and (2.19) we get

$$d - d_o = \tfrac{1}{4}d(\Delta V/V \,.\, D/d) \tag{2.20}$$

This implies that if the dynamic range (i.e. D/d) is allowed to

approach a value of $V/\Delta V$ the spot size will increase by a quarter of its original diameter. This ratio then, would seem a good limiting value to the dynamic range. A typical value for $V/\Delta V$ is 10^4 and with this dynamic range we can define 10^8 co-ordinates when X and Y deflections are combined (assuming other aberrations are corrected).

Two further aspects of deflection systems should be mentioned here. These are the bandwidth requirements, and the degree of linearity in the steady state deflection sensitivity.

The ultimate bandwidth of the system is limited by the transit time of an electron through the field, but long before this limit is reached losses in the coil usually reduce the bandwidth. The coils should be fed from a source with high dynamic impedance (current source) as this prevents cross-coupling between X and Y coils. Due to the proximity of the metal walls of the column, the effective Q of the coils may be reduced. The effective bandwidth should be compatible with the maximum rate of change of information, and if necessary the system can be compensated by boosting the high frequency content of the deflection signals.

Non-linearity in the deflection sensitivity due to curvature of the field can always be compensated by suitably processing the input deflection signal[18]. This is particularly easy if a digital

computer process is available. In general the non-linearity is not severe for small angle deflections and may well be ignored for most EBM applications.

2.8 ASYMMETRY OF THE FIELDS

It cannot be assumed that the fields within the lenses have perfect axial symmetry. In practice very slight mechanical defects in the concentricity of the lenses and the apertures, and also misalignment of the various parts of the system along the optical axis, give rise to an imbalance of the field which causes ellipticity astigmatism. A deflection field is a special case of an imbalanced field and gives rise to deflection astigmatism (discussed in the previous section). Fortunately by careful alignment of the system, and by using a stigmator this aberration can be completely corrected.

The stigmator must introduce an equal-but-opposite imbalance of the field, and this can be supplied by a lens with quadrupole symmetry which is rotatable about the optic axis, or alternatively by an octupole lens. The quadrupole converges in one plane and diverges the beam in the perpendicular plane[19], while the octupole has effectively the same field but the crossed planes of reference are rotatable about the axis.

Figure 2.4 shows an example of a quadrupole and octupole stigmator.

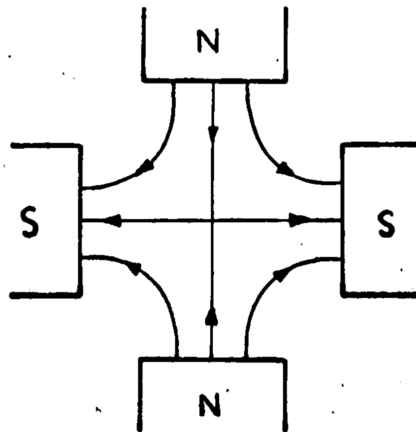

(a) Quadrupole field

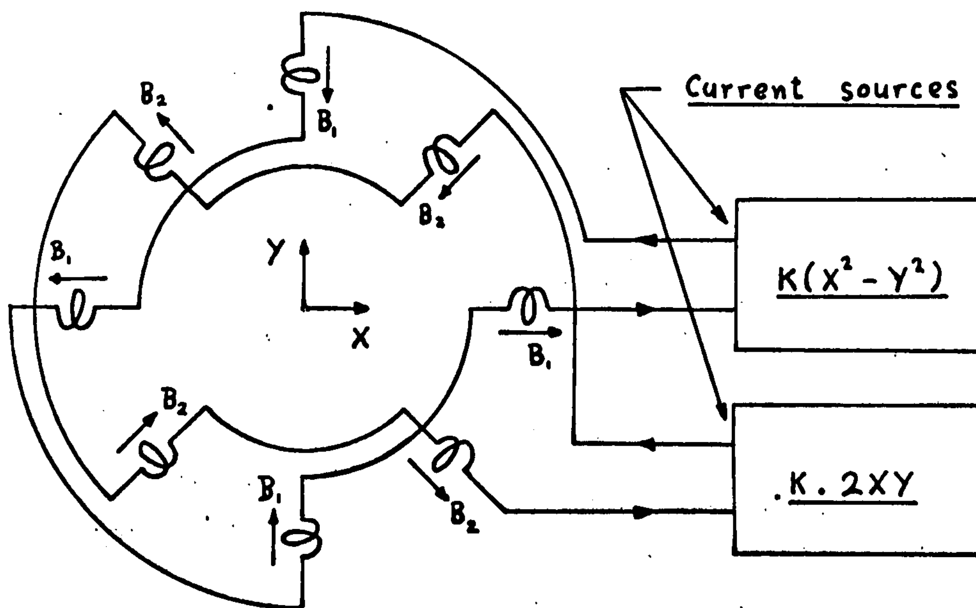

(b) Octupole system

Figure 2.4

For convenience the quadrupole field can be provided by the same coils as the deflection field, since the fields are of the same general form. It is only necessary to ensure no interaction between the stigmator and deflection signals, by using a suitable arrangement of high impedance current sources. To correct astigmatism the quadrupole must be mechanically rotated about the optic axis, and so is not suitable for dynamic corrections. The octupole on the other hand, is readily adapted for dynamic correction. When correcting deflection astigmatism, the excitation currents for the octupole coils are quadratic functions of the X and Y deflections[17].

2.9 PARASITIC FIELDS

Parasitic electric and magnetic fields will cause random deflection of the beam, and will be another source of astigmatism.

Electric fields arise when electrons, either direct from the beam or scattered or secondary electrons, accumulate on any insulator in the system. If organic vapour is present in the beam column, a polymerised film is liable to form on the walls of the system, and more seriously on the apertures themselves, and this film charges up producing electric fields which usually vary in an irregular way. It is important therefore to use "clean" vacuum pumps free from oil, and to design proper sheilding for any insulators in the system.

It is difficult to completely eliminate stray magnetic fields. These fields are usually the result of transformers, motors, or bad multiple-earths, and their effect is to produce a lateral vibration of the beam which blurs the image. The magnitude of the error is inversly proportional to the velocity of the electrons and proportional to the square of the beam length. Magnetic sheilding is particularly important at the cathode where the electron velocities are low. The stray fields from a magnetic ion pump can be very strong, but since this is a stationary field it can in theory be compensated. However the most practical solution is to provide the ion pump with adequate magnetic shielding.

Another source of spurious magnetic fields arises if there are any ferromagnetic materials in the vicinity of the deflection fields. Inhomogeneity and hysteresis in the magnetic properties of the material will cause serious aberrations during deflection, so such materials are not allowable near the deflection coils.

2.10 MECHANICAL INSTABILITY

Sources of mechanical instability may either be vibration from nearby machinery (e.g. a rotary pump), or thermal migration of the high temperature tungsten filament if this is being used as a cathode.

The effect of mechanical vibrations is to produce slight oscillation of the system about the optic axis, and it is reasonable to suppose that systems with very long columns would experience greater perturbations from this effect. On the other hand a physically small system can more easily be isolated from vibration.

There are alternatives to the tungsten filament cathode which do not suffer from mechanical instability. A lanthanum hexaboride rod operating at 1600 °C has greatly improved stability[20], while a tungsten field emitter cathode has virtually complete mechanical stability. These cathodes are unfortunately prone to contamination and so require more stringent vacuum conditions, particularly in the case of the field emitter source[21]. These drawbacks will be discussed more fully in the following chapter.

2.11 THE INTERACTION AT THE WORKPIECE SURFACE

Let us now look at what happens as the beam impinges on the workpiece surface. Whether thermal machining or an electron-optical process is being used, it is found that the sphere of influence of the beam may extend to several times the original beam diameter due to dispersion of the electrons at the surface.

The primary dispersive effects[22] are penetration by the high energy beam electrons, backscattering of these electrons, and the

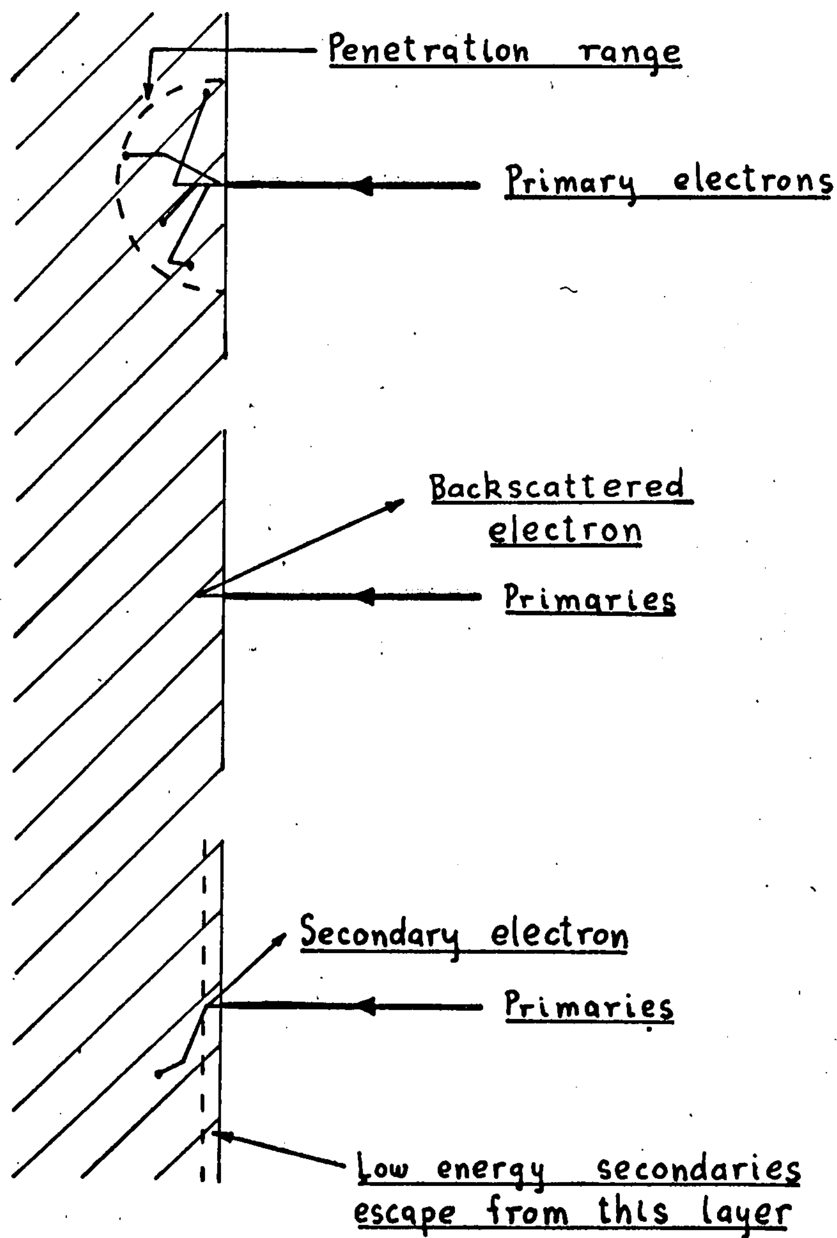

Figure 2.5 Dispersive effects at target surface

production of secondary electrons. These effects are depicted in figure 2.5. The penetration increases with the electron energy and decreases with the density of the target material. A high energy electron may be transmitted through an unsupported thin film without losing very much of its energy to the film. This means that the substrate material is important in determining the effect of scattering, since it is there that most of the beam energy is dissipated.

For the case of an electron-optical process where an insulating film is being formed, charging of the insulator will disperse the beam and may be a limiting factor for high resolution. This effect is reduced by limiting the brightness of the beam, or by increasing the beam potential. With any electron-optical process a minimum charge per unit area of target is required for effective reaction. This may vary from 10^{-1} coulombs/metre^2 to as much as 10^4 coulombs/metre^2 [23], and if the beam current is low this will result in a very long process time and consequently a build up of errors due to instabilities and drift in the power supplies.

From this it can be seen that the beam parameters must be determined by taking into account the interaction at the target surface. The highest beam current compatible with required resolution should be used, and for the optimum beam voltage scattering will impose an upper limit, with aberrations and surface space charge determining the lower limit.

CHAPTER 3

THE ELECTRON SOURCE

3.1 ELECTRON EMISSION

Electron emission from the surface of a body occurs when sufficient kinetic excitation energy is transferred to some of the outer orbit or "valence" electrons that are found near the emission surface. This permits the electron to overcome a natural potential energy barrier existing at the surface. Electrons may only increase their energy (E) if there are vacant energy levels above them, and this applies to the more energetic electrons which lie very near or above the Fermi level, so these electrons are referred to as the conduction band electrons, while electrons with lower energies lie in the valence band.

The situation is depicted in figure 3.1(a). The necessary added energy to raise one of the conduction band electrons to the vacuum level is $e\phi$ electron volts, where ϕ is called the surface potential and $e\phi$ the surface work function. The value of the surface work function is typically around 4 or 5 electron volts for pure metals. The diagram refers to a smooth, plane, metal surface, where irregularities of atomic dimensions are neglected and a uniform distribution of surface work function is assumed.

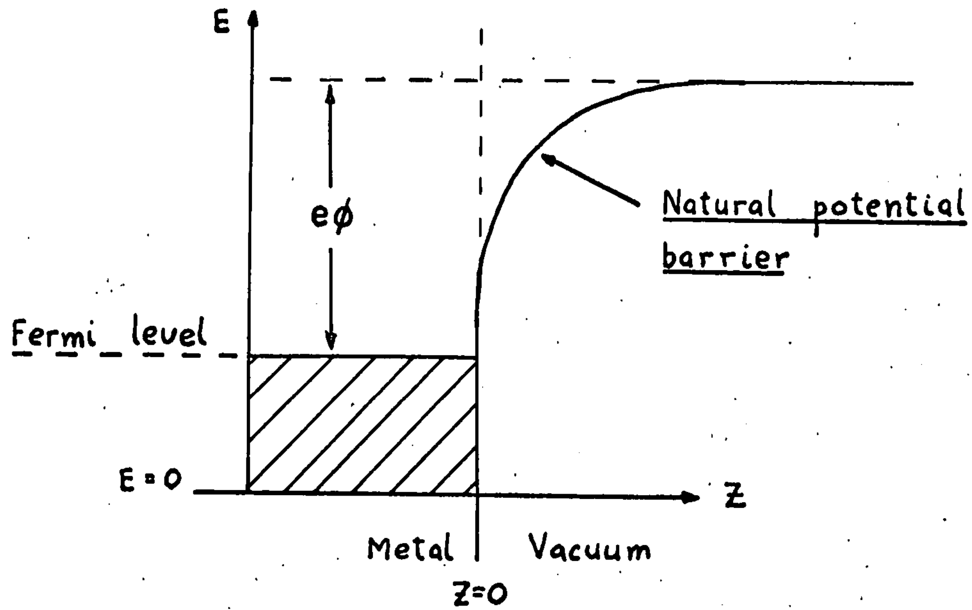

(a) Thermionic emission

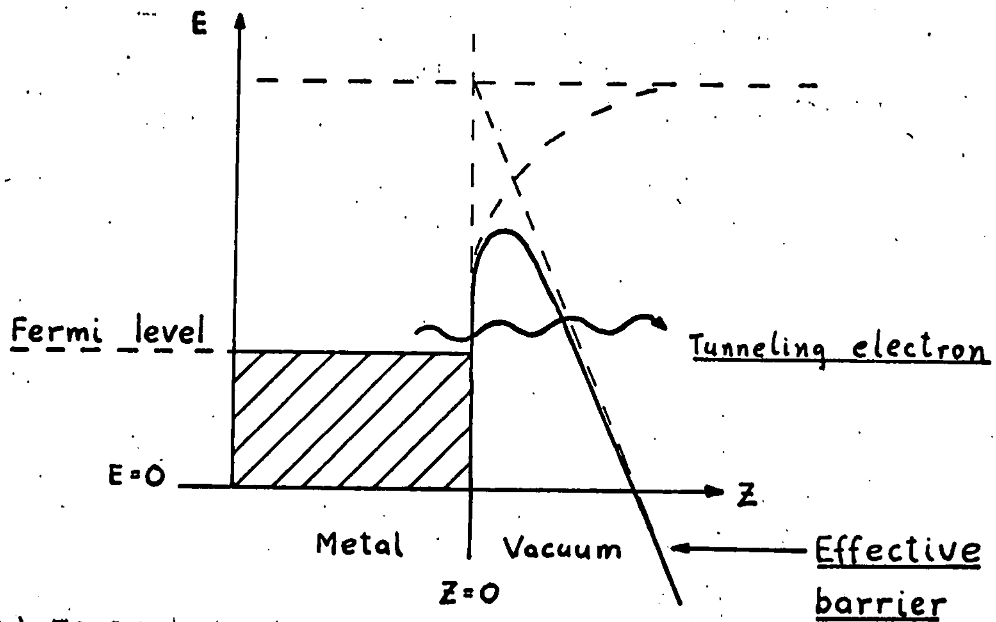

(b) Field emission

Figure 3.1 Energy diagrams

In fact it is found that even for a perfectly clean metal, the surface work function is not a constant but varies with crystallographic direction.

There are a number of mechanisms which will induce electron emission. Two basic and important types are thermionic emission and high field emission. Though some other basic mechanisms exist, they have not been developed as useful methods of producing intense electron beams.

Thermionic emission is caused by the addition of energy to the free electrons by means of energetic lattice vibrations that occur at elevated temperatures. A simplified form of the Richardson-Dushman equation[24] which describes thermionic emission, is

$$\text{current density} \quad J = AT^2.\exp(-e\phi/kT) \qquad (3.1)$$

where A is a constant, T the emitter temperature, $e\phi$ is again the surface work function of the material, and k is Boltzman's constant.

When an electron-accelerating field is applied, an additional mechanism is present which increases the normal thermionic emission current. This is called the Schottky effect, and the increased current is explained by the fact that the surface potential barrier is reduced by the applied field.

Field emission is quite different from thermionic emission, and to explain the phenomenon the wave nature of the electron must be considered. A result from quantum mechanics predicts that an electron can penetrate or tunnel a limited distance into a potential barrier. The mechanism of high field emission depends on the ability of a small proportion of the electrons to tunnel the barrier at the surface (figure 3.1(b)). In the presence of very high field strengths (above 10^9 volts/metre), the natural potential barrier is not only somewhat reduced but also thinned, so electrons have a finite probability of tunneling right through the barrier. Nordheim and Fowler have derived an expression for the emitted current density caused by high field emission. A simplified form of their equation is[24]

$$\text{current density} \quad J = AE^2\phi^{-1}.\exp(-B.\phi^{\frac{3}{2}}.E^{-1}) \qquad (3.2)$$

where A and B are constants and E is the value of the electric field at the surface.

3.2 THERMIONIC VERSUS FIELD EMMISION

The choice of cathode material and emission mechanism considerably affects the design of the electron source, and indeed the general design of the whole system. It will be instructive to compare the characteristics of the following selection of four diverse types of cathode.

i) The tungsten hairpin filament. This is the most common type of cathode used in all types of demountable vacuum systems. The filament is typically 0.1mm. diameter, bent into a "V" with the point placed on the axis, and it is normally only the point that emits. The working temperature is usually around 2700°K.

ii) Lanthanum hexaboride (LaB_6). A recent paper by Broers[20] describes the operation of a solid rod of LaB_6 which is indirectly heated and operates at 1760°K.

iii) Tungsten needle (field emitter). Tungsten can be formed into needles with tips down to 0.1 micron radius (see section 3.3). The high fields required for field emission are easily obtained at the tip.

iv) Heated tungsten needle. It is sometimes an advantage to operate the tungsten needle source at elevated temperatures (e.g. 2000°K). At this temperature thermionic emission is low for tungsten but the strong field at the tip induces Schottky emission.

The importance of high source brightness was emphasised in the previous chapter (section 2.6). Brightness is related to the emission current density and also to the energy spread or coherence of the emitted electrons. Very high current densities are possible with tungsten field emitters because there is a very small emitting

area. Field emission is very sensitive to changes in work function which in turn alters slightly with crystallographic direction. Consequently the best results are obtained with single crystal emitters oriented to produce intense axial emission, e.g. having the plane with Miller indices <310> perpendicular to the axis[25]. Dolan and Dyke[26] have studied the energy distribution of electrons emitted from metals for various combinations of temperature, applied surface electric field, and work function. Some difference exists in the range of energy distribution half-widths for field and thermionic emission, so to obtain a more coherent source either field emission or low temperature thermionic emission (below $2000^{\circ}C$) is preferable.

Everhart[14] has recently analysed the theoretical performance of crystal point cathode sources, and estimates that a cold field emitter has 10^4 times higher brightness than a comparable Schottky emission cathode, which in turn should have approximately 100 times the brightness of the conventional hairpin cathode or the LaB_6 cathode. Moreover, Crewe et al.[27] have furnished experimental evidence of the great improvement in intensity that can be obtained from a tungsten field emitter. There is little doubt that if properly utilised, the field emission cathode gives much better brightness than any of the other three types of cathode.

As far as electrical stability is concerned the order of merit is

reversed. The tungsten hairpin filament is stable in relatively poor vacuums (10^{-3} to 10^{-5}Torr) and also in the presence of oil and water vapour. These are the conditions that obtain in the great majority of demountable vacuum systems. To some extent this also applies to the LaB_6 cathode, though Broers quotes a vacuum of 10^{-6}Torr for his experiments. Other thermionic emitters such as the oxide-coated and dispenser types are rapidly "poisoned" under these conditions. Conventional vacuums are also suitable for heated tungsten needle or Schottky emitters(28). The main problem with field emitters is that they are prone to contamination and are consequently unstable except at ultra high vacuums. Satisfactory operation at pressures of 10^{-9}Torr are reported and at present this seems the limiting pressure at which field emission is useful.

Cathode life is yet another important consideration. For thermionic cathodes the ratio of electron emission rate to material evaporation rate effectively determines cathode life, and for tungsten this ratio is rather low. Bloomer(29) reports an average life of thirty hours for a 0.005" tungsten hairpin at emission densities of $3A/cm^2$, but at the same emission density the LaB_6 cathode, operating at 1760^oK, has an estimated life of 8000 hours. For field emitters the life is determined mainly by the rate of sputtering of the emitter surface, and this is governed by the emission current as well as the operating pressure. At very high vacuum (10^{-12}Torr) emission is substantially constant for many thousands of hours. At 10^{-9}Torr

the average operating period is one hour, however the tip may be reconditioned in situ by "flashing" at a high temperature and also (if desired) by applying a positive voltage to the tip during flashing. It is in theory possible therefore, to operate field emitters for unlimited periods if due precautions are taken and the tip periodically reconditioned. The stability and life of heated field emitters or Schottky emitters have been investigated in detail by Dyke et al.[28]. They found that such emitters have an optimum operating temperature for prolonged life in vacuums of 10^{-6}Torr, and that the major cause of failure was impurities in the cathode material migrating to the emitting surface and initiating a vacuum arc.

Mechanical instability for these four cathodes is only a problem with the tungsten hairpin filament. Again this is due to the high operating temperature and relatively high evaporation rate.

The different mechanical complexity of the four cathodes is worth considering. Broers' electron gun is the most complex since he had to incorporate a high powered radiant heater for the LaB_6 rod. On the other hand the field emitter gun should be the simplest to construct. It has great mechanical stability, small size, and does not require a continuous filament supply at EHT.

In view of, or perhaps in spite of all the above considerations,

I have adopted an electron gun design based on a tungsten field emitter for the experimental EBM. The necessary additional cost of a UHV system is an undoubted disadvantage. To offset this, reductions in the size and complexity of the vacuum system are being tried. Two features which recommend field emission for an EBM system are first, very high brightness and second, mechanical stability and prolonged operation. I feel that ultimately this type of gun can be designed to operate with a minimum of maintenance and adjustment, and is thus well suited for use in a fully automated EBM system.

3.3 FABRICATING THE TIP

Because of the very limited use of field emitters, standard tip assemblies are not yet manufactured and users have generally no recourse but to make their own. In a sense this is an advantage, since the tip is a very delicate structure and least risk of damage results if handling is minimised. A good practice is to arrange that the final tip-forming etch is carried out with the gun fully or partly assembled, and just prior to its installation in the vacuum system.

Tungsten is the most popular material for field emission work. It has a high melting point, good electrical and thermal conductivity, and high mechanical strength. The technique of fabricating

the tip has been outlined by Dyke and Dolan[30], and various authors have added their own variations to this technique. I will here include an account of the techniques used in this instance.

The tip is welded onto a filament, and high purity 0.5mm. annealed tungsten wire is used to make both the filament and the tip. A 5mm. stub is first spot welded onto the filament, which is simply bent into shape to the approximate dimensions shown in figure 3.2. To ensure good concentricity the tip is welded onto the filament using the jig detailed in figure 3.2. Because of the fibrous nature of annealed tungsten wire and its tendency to harden and split when worked or cut, it is best to finish off the required lengths of wire by etching. To etch the 5mm. stub approximately one inch of tungsten wire is used. This is held in a 5mm. length of 1/8" diameter brass with a 0.5mm. concentric hole (a close fit for the tungsten wire) and forms one electrode, the second electrode being of nickel plated brass. Using about 6 volts AC , the excess is etched away leaving 5mm. inside the brass electrode. To finish off the filament the ends are immersed in the electrolyte with insulating sleeving giving protection up to the required length, and again an AC etch is used to remove the excess from the ends. The electrolyte used to etch tungsten is a one normal solution of sodium hydroxide (NaOH).

Before the needle is finally formed, the stub and about 10mm. of

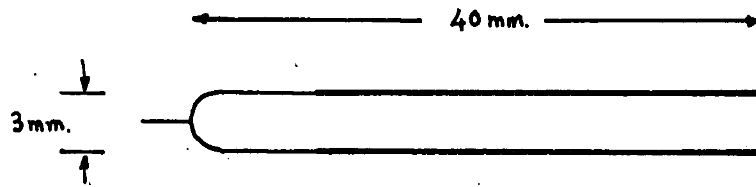

(a) Filament and stub before final etch

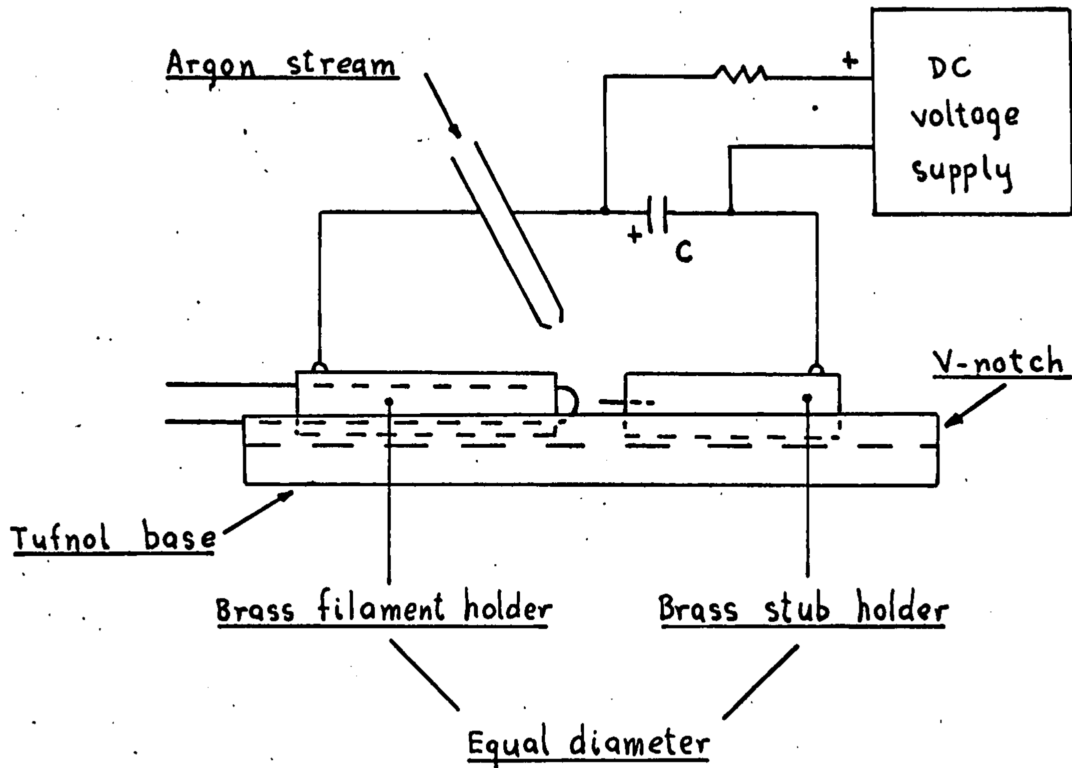

(b) Capacitor-discharge welding jig

Figure 3.2

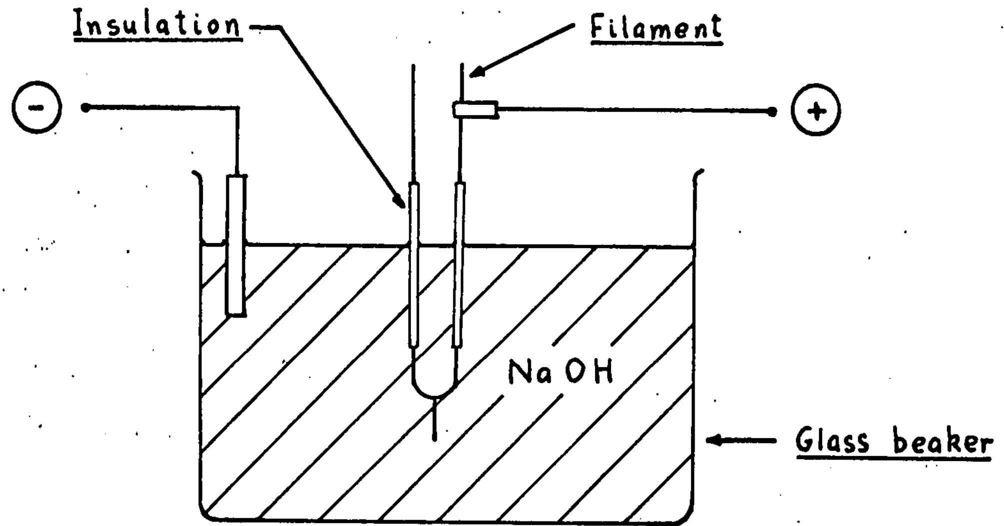

(a) Pre-forming etch

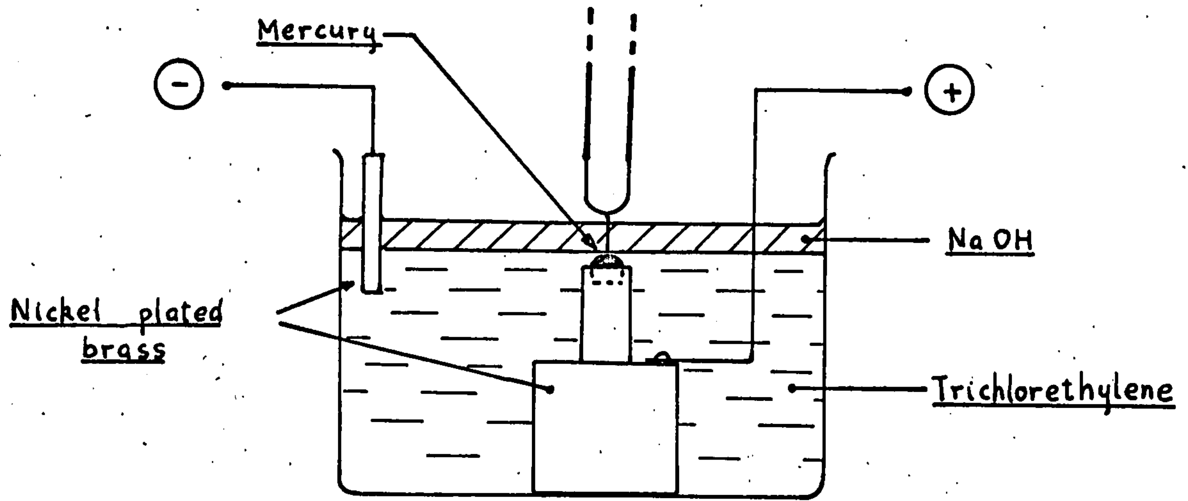

(b) Etching the needle

Figure 3.3 Etching methods

the filament are etched down to a diameter of approximately 0.2mm. using 10 volts DC and with the electrolyte arrangement shown in figure 3.3. This DC etch also polishes the filament and stub. To form the needle, a special electrode has been devised which supplies current to the tip of the stub via a small pool of mercury (see figure 3.3). The mercury and tip are just immersed in trichlorethylene, and the electrolyte floats on top of this. Two methods of etching the needle are possible using either an AC or DC etch. The first method, using 6 volts AC, preferentially etches about half-way down the electrolyte layer. A neck is formed in the stub and eventually it parts in two, at this point etching ceases and the needle formed is 1 to 2mm. long with a fine taper. With the second method (10 volts DC) necking occurs at the electrolyte meniscus, and the needle can form very close to the filament with an acute taper. So far experiments have been carried out using only the first type of needle, but the second type should provide a better thermal conduction path from filament to needle tip, so this type will be used in subsequent experiments. The voltage settings quoted above are arbitrary and may be varied to some degree. Excessive voltages cause too much turbulence and heating, while lower voltages result in longer etching times. It was found experimentally that a co-relation exists between the etching voltage and the needle taper, and it would be an interesting study to establish the quantitive laws relating tip geometry with voltage and current.

EX BIBL UNIV EDINB GEN

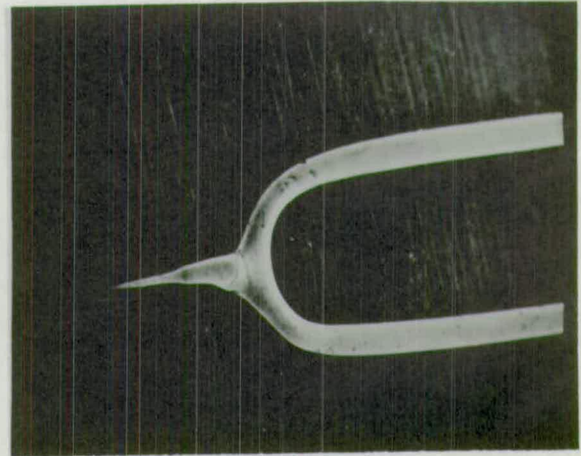

(a) First type

(20x)

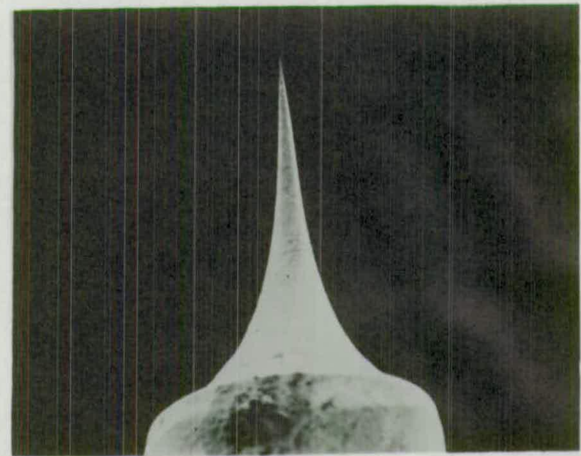

(b) Second type

(200x)

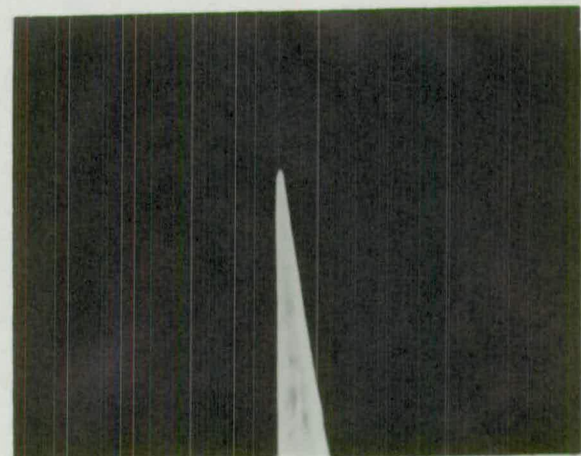

(c) Second type

(2000x)

Figure 3.5 Field emitters

The tungsten wire for both filament and needle has been a poly-crytalline grade, as this is very much cheaper and easily available. After the electron gun system has been fully tested and modified it will be necessary to obtain some <310> oriented tungsten wire with which to make the stub.

3.4 FIELD EMISSION EXPERIMENTS

Before experiments were started with field emission tips, some thought was given to the design of the EHT supply with which they would be operated. A feature of previous reports on field emission was that the life of each emitter was strongly dependent on operating pressure, since ionic bombardment of the emitter surface appears to be the main cause of failure[21]. When the surface is sputtered in this way the original smooth radius becomes irregular and emission high spots occur, eventually leading to cathode destruction. In all the experiments which have reported this phenomenon the emitters have been operated with a constant applied voltage. The alternative of using a current source capable of operating over several kilovolts seemed to offer interesting possibilities, since this type of source would limit the total energy of sputtering ions at the emitter surface.

Figure 3.5 shows the main elements of two circuits capable of

a high degree of current regulation. Both circuits have been designed round the 7235 high voltage triode, manufactured by the Victoreen Instrument Company. The power source was in both cases a Brandenburg model 705 regulated high voltage supply. Because of the high gain of the 7235, the transistors in these regulators need only have 30 volt ratings, and in fact these hybrid circuits have been continuously operated for several hundred hours without breakdown.

The first circuit supplies a simple two electrode system, comprising the field emitter needle and a single plate anode which was made of molybdenum. The needle was not a filament mounted design for this initial experiment, but was simply a length of 0.5mm. tungsten etched to approximately 1 micron radius and mounted 3mm. from the molybdenum plate. The current collected by the anode was measured on a Keithley type 610B electrometer, while the voltage was monitored on a TOA Electronics model EPR-2TD pen recorder using a chart speed of 20mm. per hour. The field emitter assembly was mounted in the UHV system which had a sorption roughing pump and an 8 litre/sec. getter ion pump attached (see figure 1.3). After initial pumping and a bakeout at about 200°C for 24 hours, the pressure was pulled down to below 10^{-9}Torr. This bakeout was the only de-gassing treatment available for the needle and anode. Flashing the needle at 2000°C is usually recommended as necessary to obtain an uncontaminated smooth emitting

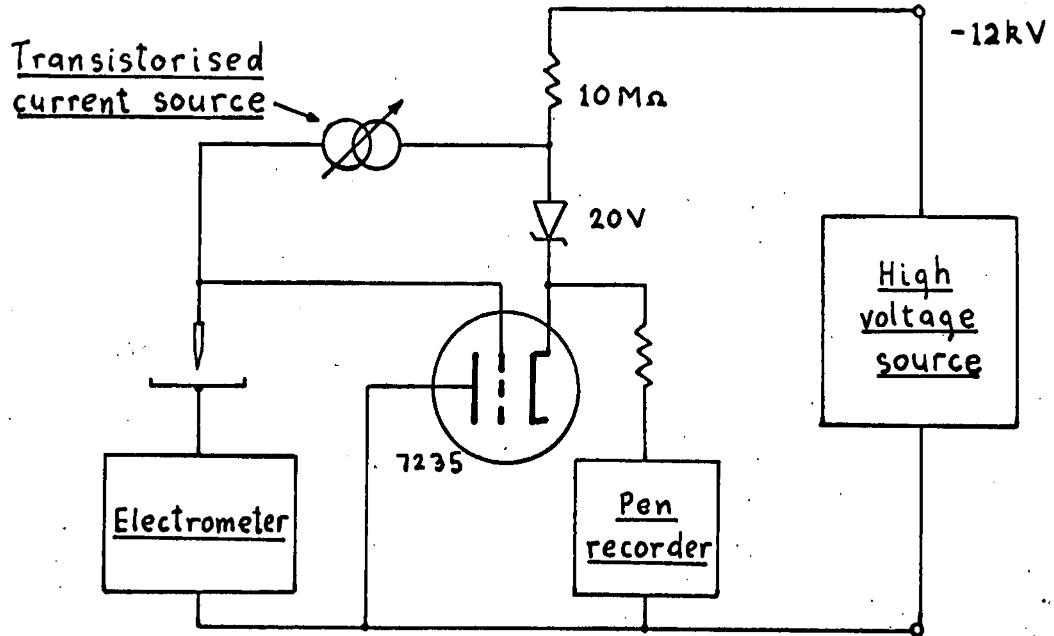

(a) Two electrode controller

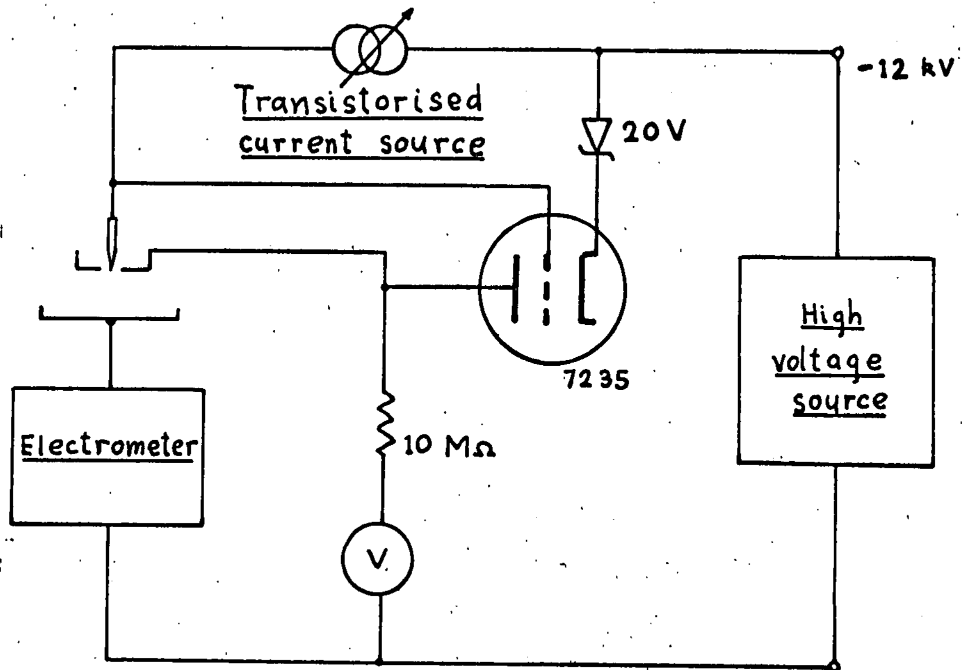

(b) Three electrode controller

Figure 3.5

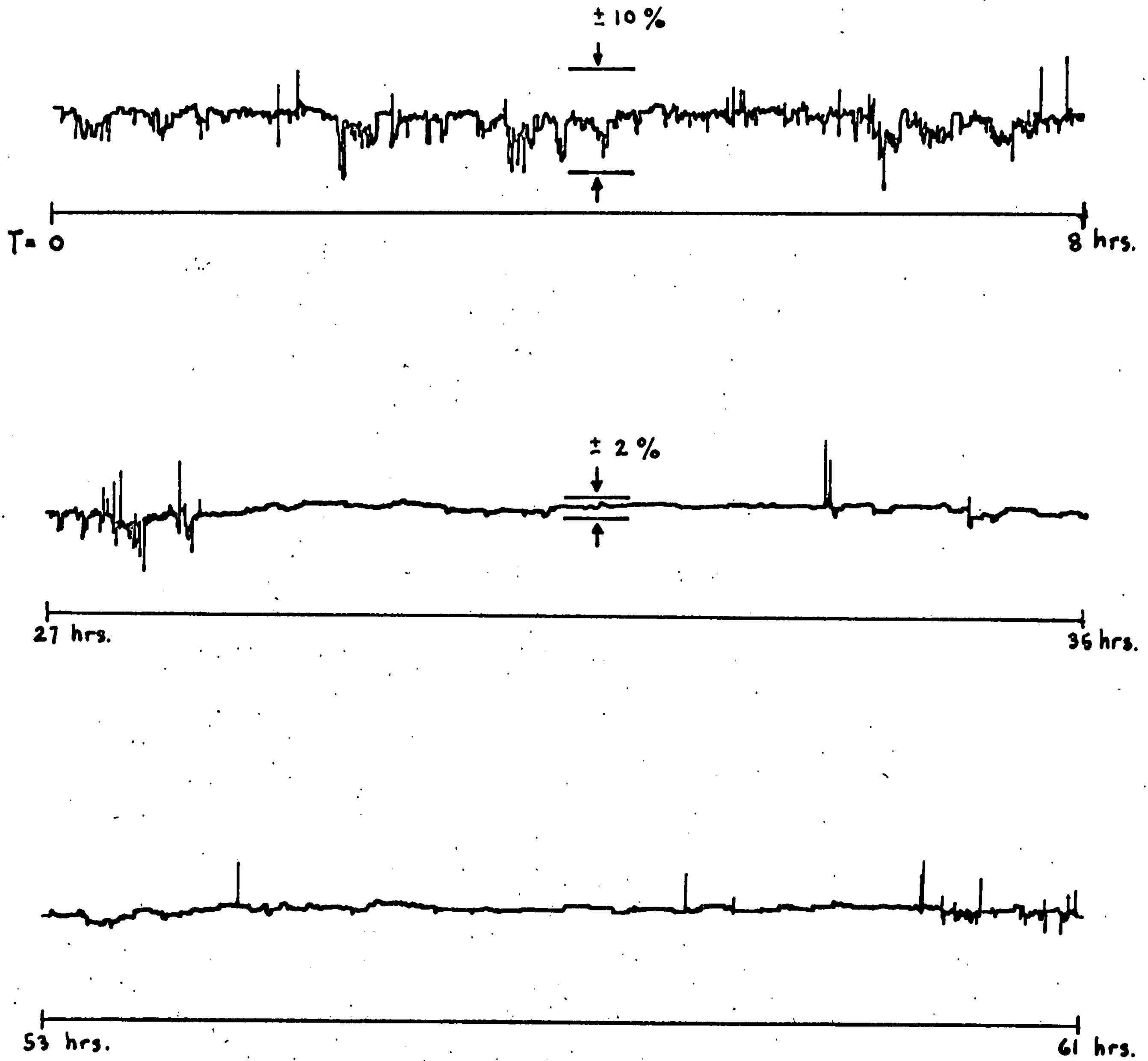

Figure 3.6 Pen recorder trace

surface, so this experiment was carried out with a "raw" contaminated needle. The current from the needle was variable from 1 to 20μA and tests showed that DC regulation was within 1% from 500 volts to 10 kilovolts (negative potentials).

The current was set at 5μA and the electrodes connected. Initially the voltage stayed at 12kV and only a few nanoamps registered on the electrometer. The current gradually increased to 5μA and at the same time (after about 30 minutes) the voltage settled down to 1.7kV. With the increase in current the pressure in the system rose to 5×10^{-8} Torr, due to electron bombardment and outgassing of the anode. During this first 30 minutes ion bombardment had radically changed the emissivity of the cathode. The high initial voltage suggests that a substantial layer of contaminant had increased the effective surface work function. Sputtering would have partly removed this as well as increasing the surface roughness, and this caused the observed decrease in impedance of the "diode" arrangement.

It is very interesting to note what happened for the remaining 100 hours or so of the experiment. Figure 3.6 shows a copy of part of the pen recorder trace. The mean voltage remained at 1.7kV for the duration of the experiment, but as can be seen, the instantaneous voltage fluctuated randomly. For the first 28 hours this fluctuation was fairly continuous, and the maximum deviations

from the mean were about ±10%. After this there was a long period where the emission behaviour was much more stable, with periods of up to 30 minutes when the measured voltage was substantially constant. Later on (at 60 hours) unstable behaviour again set in, but before the trace ended another shorter period of stable emission occurred. The experiment was prematurely curtailed after about 100 hours due to the breakdown of the high voltage power source. During the experiment the DC current was a constant 5μA, but since the regulator did not cope with transient changes in load, there was a small AC component superimposed. It is unfortunate that a continuous trace of other parameters such as transient current and pressure was not arranged. This information, along with measurements of the residual gas composition and scanning electron microscope monitoring of the tip geometry, may well give answers to why this pattern of stability occurs.

Periodic checks showed that the pressure did not vary to any extent from $5x10^{-8}$Torr throughout the experiment. Using a constant applied voltage, the lifetime of a tungsten needle under these conditions is generally reckoned to be of the order of one minute, due to the regenerative breakdown described by Martin et al.[21]. But it is apparent that continuous operation at relatively high pressures is possible if a high performance current source is used. It appears from the trace that an equilibrium impedance exists, and it is noticable that changes increasing the impedance

are infrequent and of short duration compared to fluctuations below the equilibrium impedance.

3.5 THREE ELECTRODE CONTROLLER

The second regulator circuit allows the emitter to stay at a fixed voltage and controls the emission by modulating an additional electrode (the first anode) while the second anode is at ground potential. This forms the basis of the electron gun which will be described in the following chapter.

A full circuit diagram of the regulator in its final form is shown in figure 3.7. This circuit includes some additional functions not yet described. There are three current ranges, namely 1, 10, and 100μA, and continuous control from zero to full scale is possible for each range. A special feature is that changing range and controlling current level is done by signals at ground level. This anticipates the stage when automated or computer control will be used, rather than manual control. The range change switches are miniature dry reed types, actuated by coils at ground potential. Insulating these coils to 20kV or so is a simple matter. To provide continuous modulation of the emission current, V_s is controlled in response to a signal V_m at ground level. A current V_m/R_1 is fed to the high voltage capacitor C_1 via T_1, and this current is chopped by the unijunction

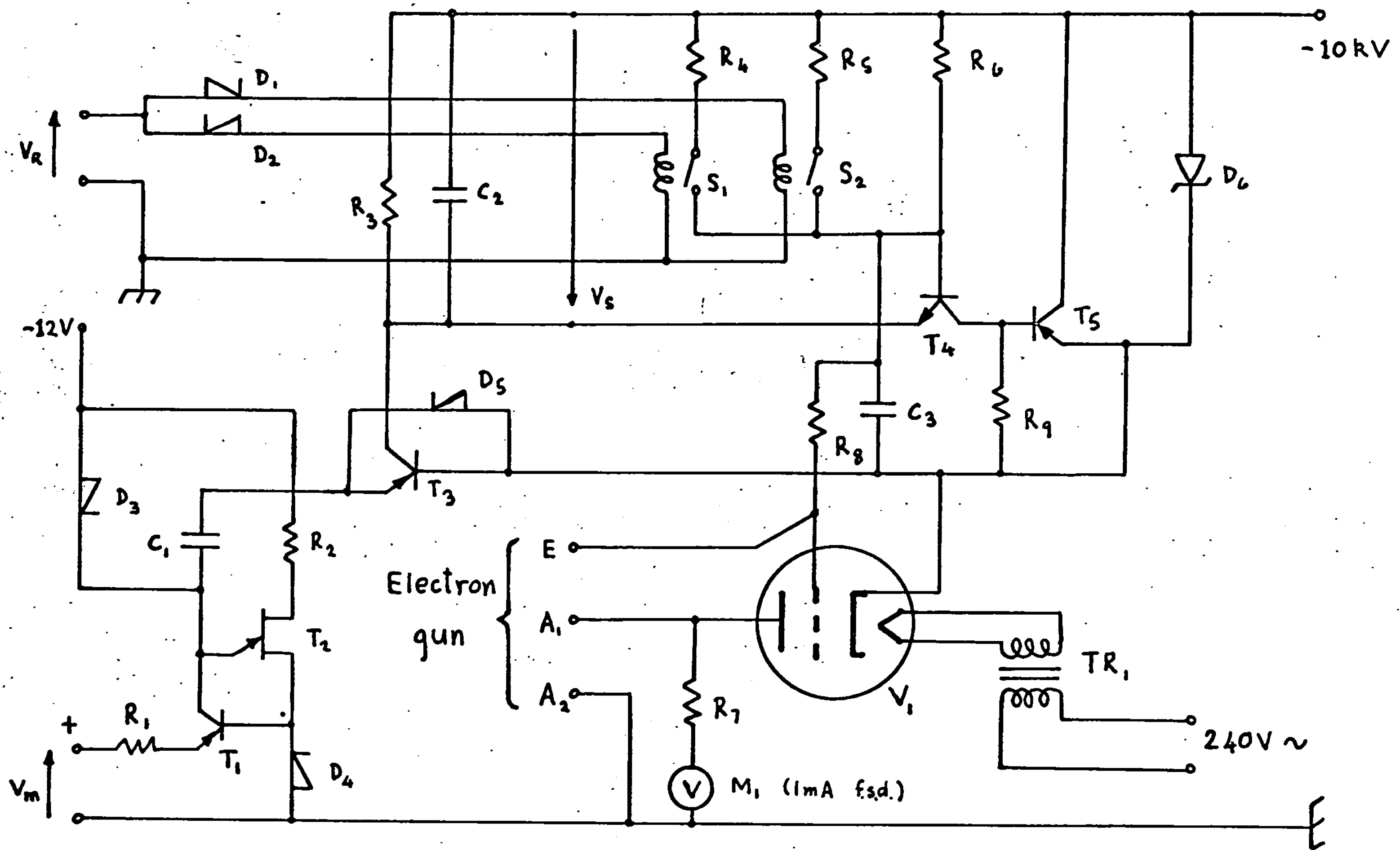

Figure 3.7 **Circuit of three electrode controller**

C_1	0.01 μF	Paper 20kV DC Wkg.
C_2	0.1 μF	polystrene
C_3	47 pF	polystrene
D_1 to D_4	1S920	silicon diode
D_5	IN914	fast recovery
D_6	HS240	24 volt zener
R_1	10 kΩ	5% hystab
R_2	33 Ω	5% hystab
R_3	6.8 kΩ	5% hystab
R_4	68 kΩ	5% hystab
R_5	680 kΩ	5% hystab
R_6	5.6 MΩ	5% hystab
R_8	10 kΩ	5% hystab
R_9	68 kΩ	5% hystab
R_7	9.4 MΩ	20 x 470 kΩ carbon comp. 2W
S_1, S_2	MSRG-2	Dry reed Insulated to 20kV
T_1, T_3, T_5	2N4058	Low level silicon PNP
T_2	T1S43	Unijunction
T_4	2N3707	Low level NPN
TR_1	"special"	Secondary 6.3V 0.5A with 10kV insulation
V_1	7235	High voltage triode

Table 3.1 Components table for fig. 3.7

transistor T_2. This chopped signal is detected by T_3 and D_5 and finally the voltage V_s equal to $(R_3/R_1)V_m$ is obtained. This simple circuit is effectively a DC to DC converter with high input/output isolation and a bandwidth of about 1kc/s. The emission current is fed through the selected combination of R_4, R_5, and R_6. T_4 compares the voltage across these reference resistors with the voltage V_s, and via T_5 modifies the cathode bias of the valve and in turn its anode potential, so that it adjusts to stabilize the current through the load. The capacitor C_3 is included to eliminate high frequency instability in the feedback circuit, and to reduce very high transient emission currents the resistor R_8 is connected in series with the primary current controller, and reduces transients to about 1mA.

In addition to this, a special ripple smoothing circuit has been inserted between the primary high voltage supply and the regulator. The supply was found to have ripple of 4 volts peak to peak with a substantial 50c/s component (at 10kV). Although this is less than 0.1% it is sufficient to cause spot defocussing and deflection errors. The circuit (figure 3.8) is basically an RC smoothing circuit with a Darlington transistor pair providing impedance conversion to decrease the DC regulation. The RC time constant for low frequencies is 0.1sec., while the DC regulation is R_1 divided by the DC current gain of T_1T_2 (approximately 1kΩ). The zener diode Z_2 which biases the collector-base voltage, should

have ultra low leakage or pre-regulation current, and the zener voltage must be slightly greater than the value of peak-to-peak input ripple. Z_1 is a 15 volt zener which protects against high voltage transients. Using this circuit the ripple has been reduced to 1ppm. (10mV) which does not contribute significantly to chromatic aberrations.

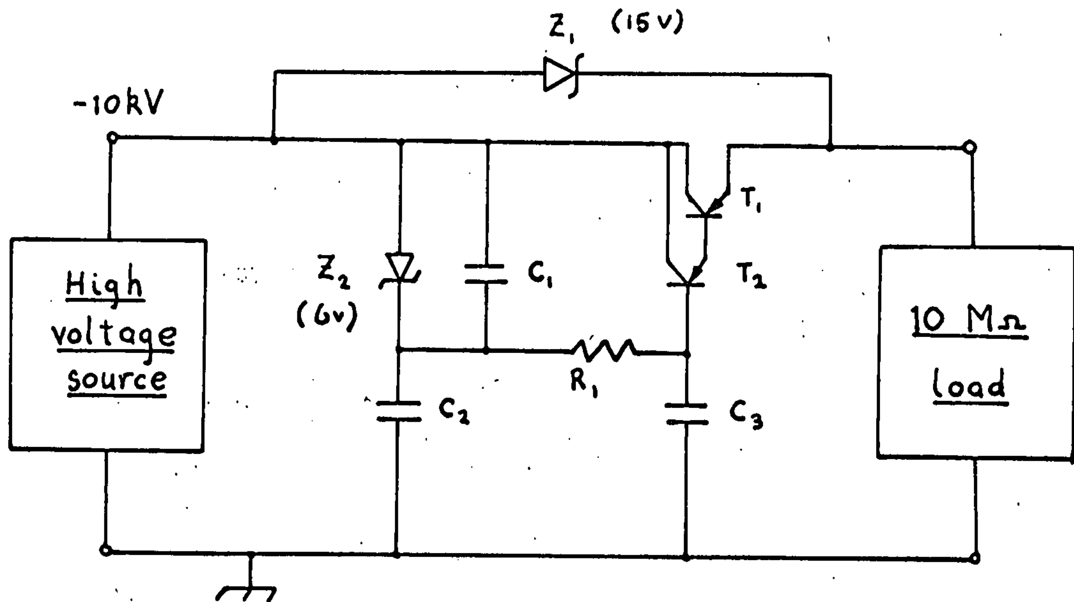

Figure 3.8 Ripple filter circuit

T_1, T_2 - 2N4058 (Texas)	R_1 - 10MΩ ±10% ½ W.
Z_1 - 1S2150 (Texas)	C_1 - 0.05μF Polystrene
Z_2 - 2N4058 base-emitter (reverse biased)	C_2, C_3 - 0.01μF 15kV DC Wkg. (TCC CP58WO)

Table 3.2 Components table for fig. 3.8

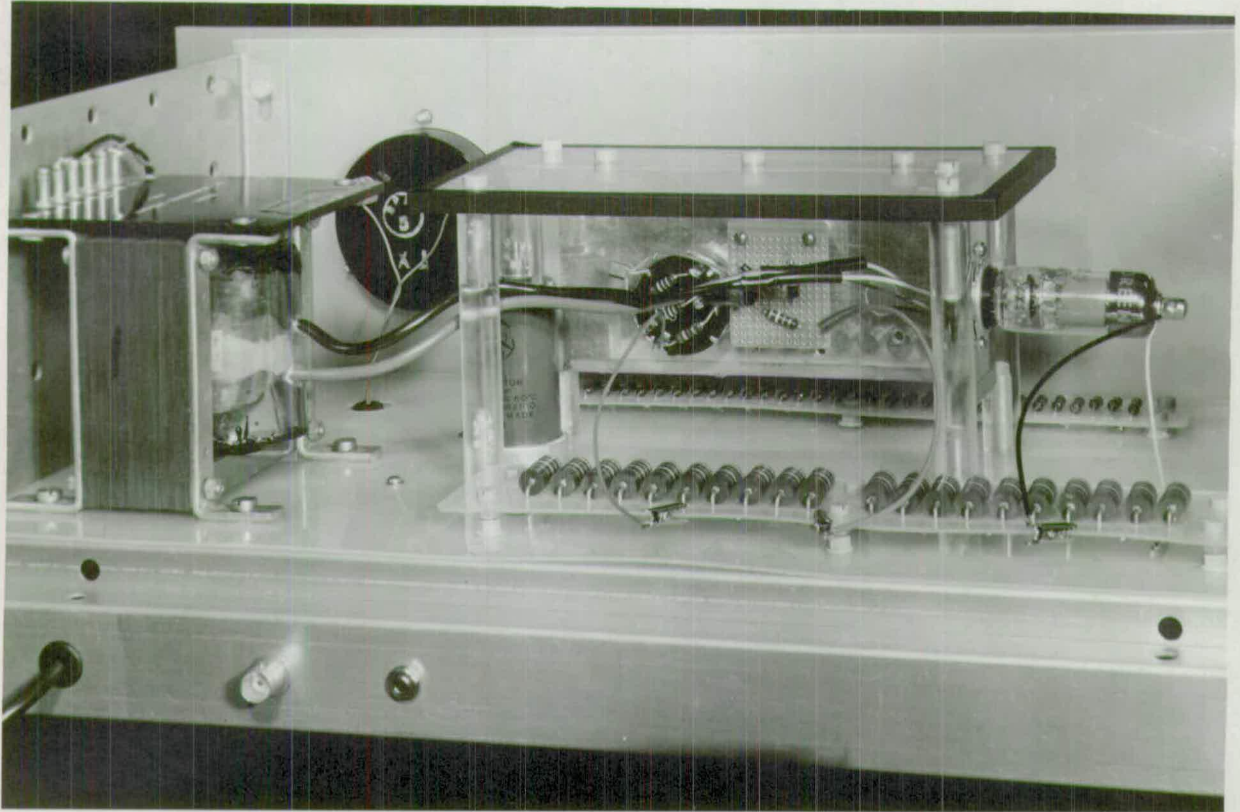

Figure 3.9 Inside view of current controller

CHAPTER 4

FORMING THE PROBE

This chapter describes preliminary attempts to form an electron probe using a three electrode field emitter gun, and a simple single lens system. The experiments carried out show that several improvements are necessary, and so a more refined system has been devised and its performance predicted. The reconstruction of the probe forming system has yet to be completed, so an account of its measured performance cannot be included.

4.1 SYSTEM N° 1

The basic features of the design are shown in figure 4.2. There are three points where this system differs markedly from a conventional system using a tungsten filament emitter.
These are :-

i) No condenser lens.
ii) No iron shielded lenses.
iii) Permanent alignment.

The role of the condenser lens in electron probe devices is to alter the demagnification of the illuminating source prior to final focussing, which has the effect of controlling the probe

current. This is demonstrated in figure 4.1 where the first two diagrams refer to a two lens system using a tungsten filament source. The illuminating source is effectively the first crossover at the electron gun. To obtain the best brightness the filament must operate at maximum emission, so the current density and convergence at this crossover is fixed. In the first diagram demagnification is high, the current density in the second crossover is increased (see section 2.6), and the current transmitted through the aperture stop is small. The second lens is illuminated by a high current density source with very small convergence, and the probe formed has high resolution and low current. With low demagnification, the effective illumination of the final lens is much greater and the probe has high current though with less resolution.

The last diagram on figure 4.1 refers to a single lens system with a field emitter source (which is assumed to be a high intensity crystal oriented type). The effective source radius is so small that no demagnification is needed, and the final resolution is a function of lens aberrations rather than the electron source[14]. It is convenient to use very small aperture optics with a single lens system which allows a very high degree of resolution, yet at the same time relatively high probe currents. The probe current can be controlled by varying the cathode emission, which is done very effectively by the instrumentation described in the previous chapter.

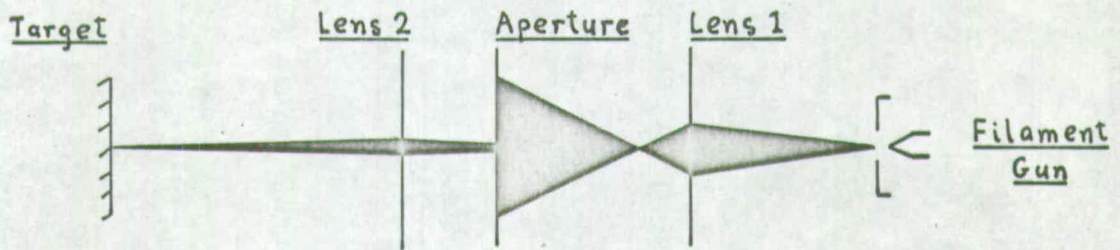

(a) High demagnification

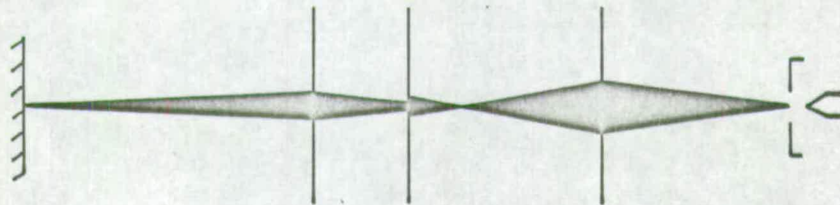

(b) Low demagnification

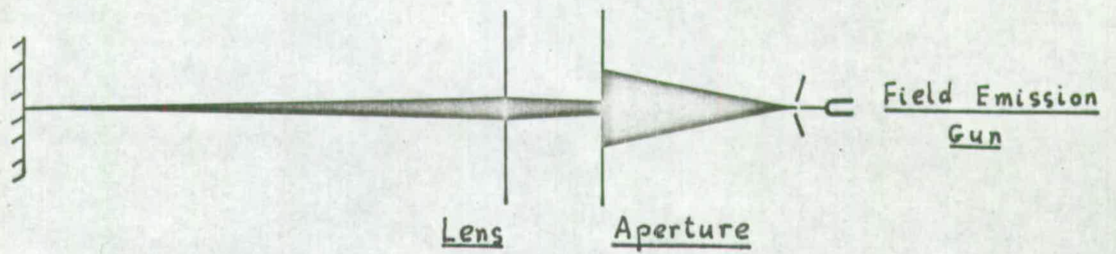

Figure 4.1 Probe forming systems

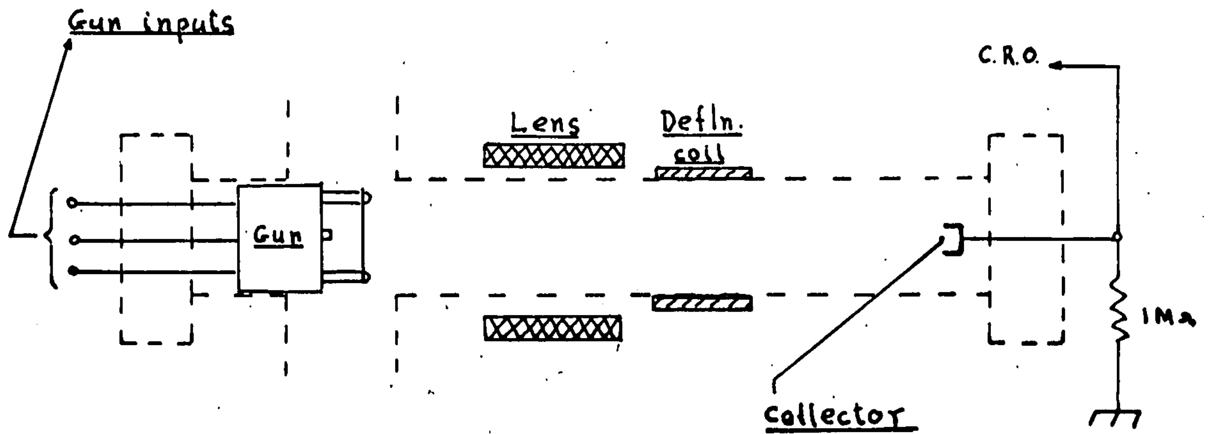

(a) General arrangement

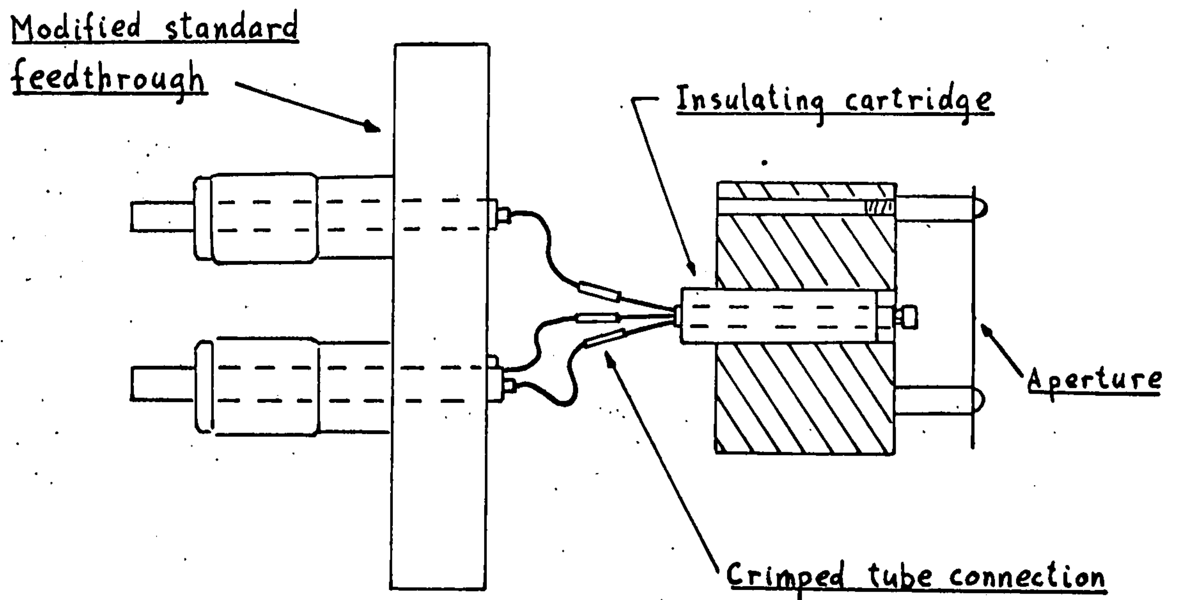

(b) Full-scale details of gun

Figure 4.2 System No 1

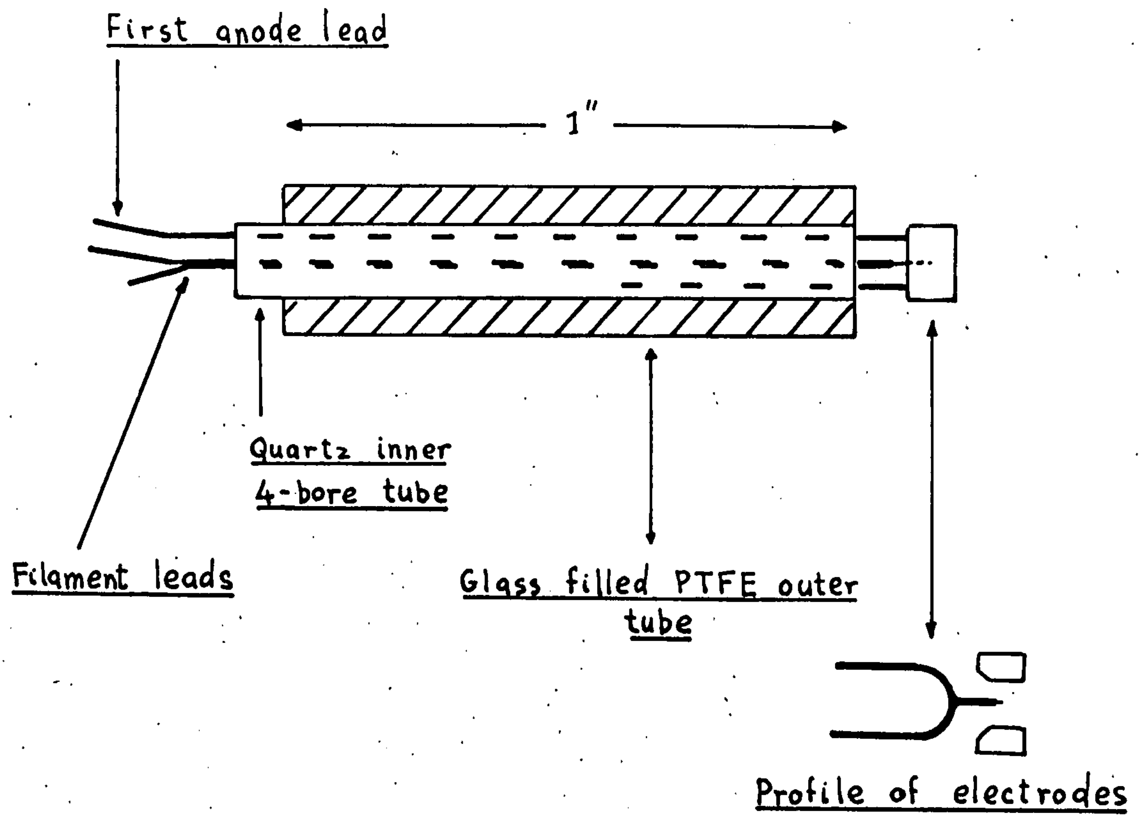

Figure 4.3 Details of cartridge

The lens used here (figure 4.2) is an unshielded solenoid type. This is much better for an application requiring relatively long focal length, low voltage beams, since a lens with iron pole-pieces would operate as a weak lens with low excitation, and this may introduce severe aberrations. The solenoid was made with a 2" bore, 2" length, and ¼" thickness of winding, and it dissipates 6 watts when focussing a 3", 10kV electron probe (excitation 600 amp turns). Because of the wide bore, the complete lens was constructed and wound outside the column, so adjustment of its axial position and alignment is easily made.

The electrode gun assembly has three main components. First a stainless steel body to which the other components are attached. Second an insulating cartridge which holds the cathode and first anode electrodes and which is a push fit in a ¼" diameter hole down the body centre. Lastly the second anode, directly fixed to the body by three stainless steel pillars. The second anode, made of beryllium copper, has at its centre a 1mm. diameter hole and allowance is made at the fixing pillars to centralise this hole in relation to the cathode point. The separation between second anode and cathode is 10mm. so the design aperture (half-angle) for this gun is 0.05 radians.

The construction of the insulating cartridge is shown separately in figure 4.3. The outside insulation of glass filled PTFE allows

the cartridge to be a tight but sliding fit in the stainless steel body. Inside this is a length of four-way quartz capillary tube, down which go the leads of the cathode-filament assembly (see figure 3.2) and the first anode. These are tungsten leads which are crimped to short lengths of copper wire, which in turn are crimped to the terminals of a three-way UHV electrical feedthrough.

The quartz tube has the advantage of having very high dielectric strength to form an effective insulator, and also serves to hold the electrodes in fair alignment. However the dimensional tolerances of the tube were very crude so the electrodes had to be visually aligned by bending the tungsten slightly - a rather unsatisfactory procedure. It was hoped to achieve gun alignment to within 0.1mm., and for this reason the gun aperture was left fairly large (0.05rad.), but the results with this aperture could be extrapolated down to the case of high alignment and low aperture conditions.

After a 48 hour pump-down and bakeout routine, the experiment proceeded. A current of 5 amps was passed through the filament to flash the needle at about 2000°C (white heat). This value of current was arrived at by observation of an identical filament in an auxiliary vacuum system fitted with a viewing port. With the current controller set for 1μA emission, the cathode voltage was

raised to 5kV and the following observations made. 1μA emission started immediately and the first anode assumed a potential of about 3kV (or +2kV with respect to the emitter). The pressure which was originally below 10^{-9}Torr rose to 10^{-8}Torr. Measurement of current transmitted through the second anode and also probe diameter, were made by focussing this current on the collector electrode (see figure 4.2) and deflecting it across this electrode. The probe diameter was measured as 0.5mm., but the total probe current was very small (only 2nA) and this substantiated fears that some misalignment of the electrodes on the cartridge had taken place when the electrodes were being crimped to the electrical feedthrough. This had to be done with the system installed in the vacuum chamber.

At the time of this experiment a manually controlled version of the current controller was being used which had three switched current levels, 1, 10, and 100μA. Switching to 10μA emission, both the collected current and pressure rose by an order of magnitude (to 20nA and 10^{-7}Torr). At 100μA the pressure rose to 5×10^{-7}Torr, and an increase in emission impedance was observed with the first anode voltage dropping to 1kV. This "dulling" of the emitter was permanent, so that on the lower current ranges the collected current was now reduced. However the original emissivity was restored by re-flashing the needle. Figure 4.4(a) shows the collected current pattern as the probe was scanned

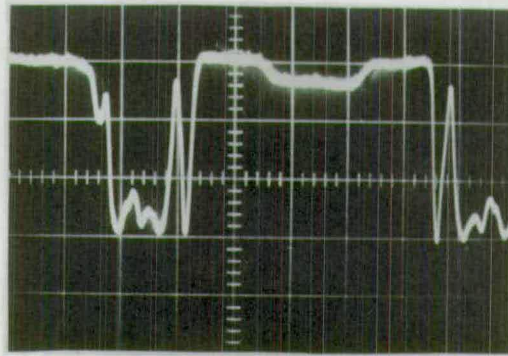

(a)

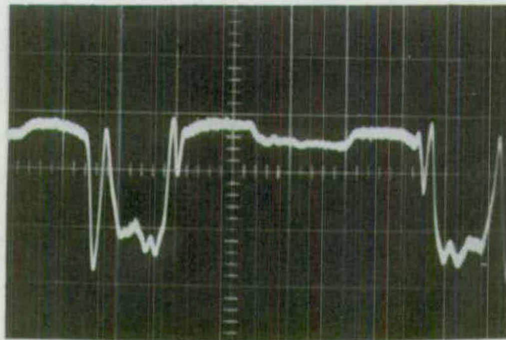

(b)

Figure 4.4 Probe currents at collector

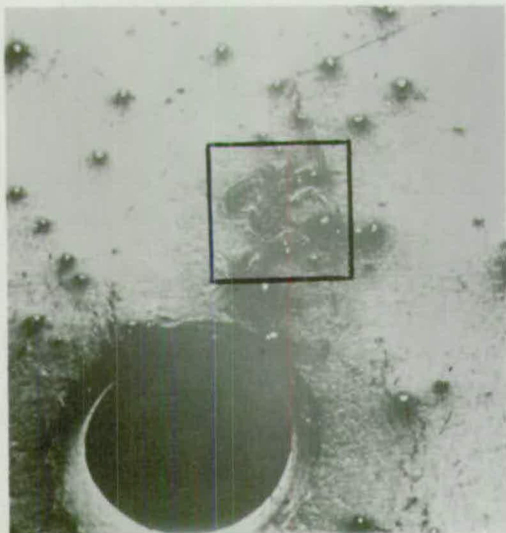

(25×)

(100×)

Figure 4.5 Aperture bombardment

across the collector before operating at 100μA. Figure 4.4(b) shows the same pattern after the dulling and re-flashing cycle. The restoration cannot easily be explained with the available evidence, since the dulling was presumably due to excessive sputtering and rounding off, of the needle tip, rather than increased contamination.

The experiment shows that continuous operation of a field emitter is possible at 10^{-7}Torr. However the pressure rise which was due to outgassing of the second anode is undesirable, since operation at these pressure levels gives rise to fluctuation in the emissivity of the cathode (see figure 3.6). After cycling back to atmosphere the gun assembly was dismantled and examined. Figure 4.5 shows scanning electron microscope pictures of the aperture area, and it is apparent that the region of high beam bombardment is displaced by about 1mm. from the centre of the aperture, indicating a misalignment of 0.1 radians in the electron-optic axis of the gun.

4.2 SYSTEM N° 2

Several things were learnt when operating the first design, and the purpose of this second design is to improve on the previous short-comings.

The aims of the new design are :-

i) To re-test the efficacy of pre-aligning the electron gun.

ii) To reduce outgassing by the beam bombardment.

iii) To use a gun aperture of 0.002 radians.

iv) To experiment with a non-focussing design for the gun electrodes.

The last two points should be explained. It can be assumed that spherical aberration was the major cause of enlargement of the focus in the original system. By reducing the aperture by a factor of 25 spherical aberration is reduced by 15,000, and it is expected that the spot diameter should also reduce by this order of magnitude. Now the residual aberrations will be astigmatism and chromatic aberration which have a first order dependence on aperture, and also diffraction aberration which is inversly proportional to the aperture.

The focussing properties of an aperture which separates two regions of different electric field are well known[31].
If the gun electrodes have focussing properties, then the effective illuminating source is either a virtual or real image of the emission surface. There are two disadvantages with this. First the image will be enlarged by aberration unless the electrodes are specially shaped, and second the axial position of the image will drift if one of the electrode potentials is not stable, (which

applies to the first anode when the current controller is used). To reduce these errors it is best to have a gun electrode arrangement that is only weakly focussing.

The design is sketched in figure 4.6. An important constructional change is the modification of the three electrode UHV feedthrough. The whole gun assembly can be rigidly fixed to the feedthrough flange, and special terminations facilitate crimping of the tungsten leads to the feedthrough electrodes. The cartridge concept is retained, but this will now be precision machined from boron nitride or some other suitable material. These changes will greatly reduce the risk of misalignment in the first two electrodes.

To reduce aperture focussing the defining aperture is placed in an almost field-free region well away from the gun assembly, and in addition two large diameter spray apertures are fitted to eliminate the transmission of reflected or secondary electrons through the defining aperture. All these apertures will be flashed in an auxiliary vacuum system prior to pump-down, since this has been found sufficient to stop outgassing[25]. The design of the first anode (see figure 4.3) is such that it collects practically no direct electron current, so it does not contribute markedly to the outgassing problem. Moreover, while it exercises very sensitive control on the electric field at the tip, it introduces no severe discontinuity on the axial potential, so

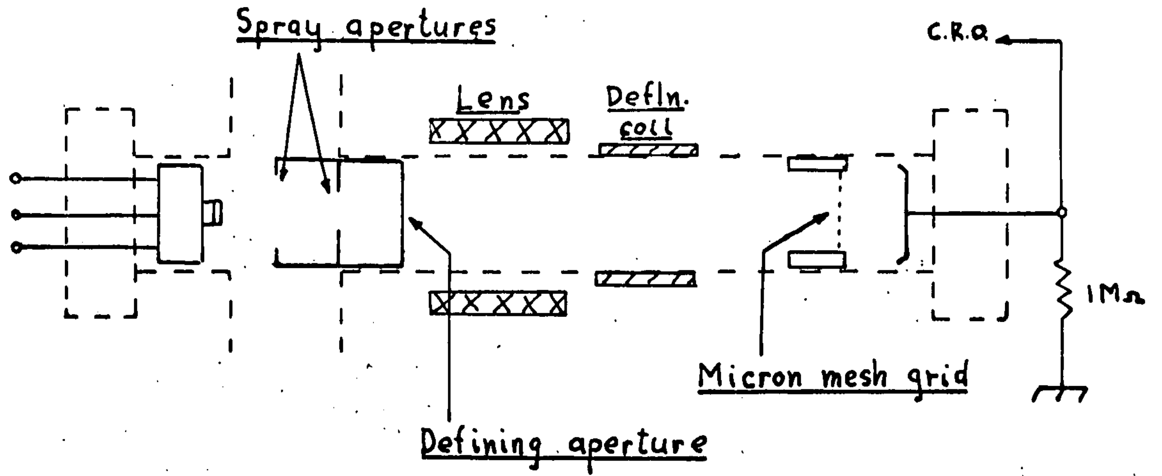

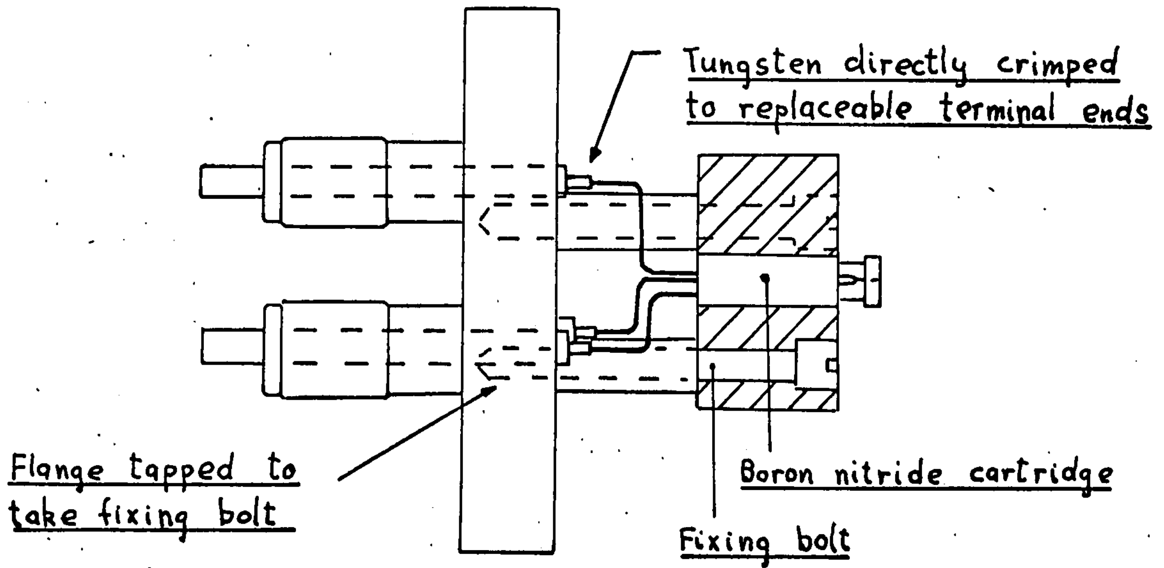

Figure 4.6 **System N° 2**

its focussing effect for paraxial rays is negligible.

The defining aperture is a 0.4mm. diameter hole 10cms. from the field emitter tip, and to ensure transmission of paraxial electrons a compound deflection-stigmator coil is placed between gun and aperture. This will effectively re-shape any bending of the electron-optical axis due to misalignment, and the deflection strength required will give an accurate indication of the amount of this misalignment.

The main deflection coil and the solenoid lens will not be altered at this stage. An additional grid aperture placed at the focal plane of the probe, with a large collector electrode behind this, will be used to study the spot size over a wide range of deflection displacements.

CHAPTER 5

THE BEAM DEFLECTION SYSTEM

5.1 D-TO-A GENERATOR

A special feature of any EBM is the system used to control beam deflection. Some of the basic modes of control have been outlined in the first chapter, and there the digital technique was singled out as being the most precise method and most suited to sophisticated automation. A major part of this project has been the designing of a high performance digital-to-analog (D-to-A) signal generator suitable for EBM applications.

Two important functions are embodied in this generator. First the design allows a very wide dynamic range in the analog output, of the order of 100,000 spot diameters. Conventional binary switched converters are limited in their dynamic range by the precision of the analog forming resistor network. Present "state of the art" D-to-A converters will resolve to 1 part in 10,000, though with advances in thin film resistor technology this figure should eventually be improved. Secondly the circuit may have multiple outputs which need not be linear functions of the input. In this way a second signal is derived which is proportional to the square of the input (i.e. the deflection co-ordinate). This is used to provide

dynamic correction of focus which is virtually essential when a large beam deflection range is used (see section 2.7)

In addition to this the outputs to the deflection coils have very high dynamic impedance (i.e. they are current sources rather than voltage sources), and also the frequency response is high. Thus transient distortion and cross-coupling between X and Y deflection coils is almost eliminated, and a high rate of information input is acceptable.

The circuit* (see figure 5.1) is designed to give a high resolution linear output current which drives a deflection coil, and simultaneously provide a voltage signal which is a good approximation to the square of the deflection current. The circuit is used in conjunction with a primary D-to-A voltage source, in this case a ladder network with a 10 volt reference supply and controlled by a 12-bit reversible binary counter. The ladder output is accurate to better than 1 part in 4000. A pulse from the final flip-flop of the binary counter triggers a reversible ring counter which selects one of four output stages. The output current is the sum of currents through the precision resistors R_{A1} to R_{A4}, summed

---

*This circuit is the subject of U.K. Patent Application No 2589/69.

Figure 5.1 Circuit for the D-to-A generator

A_1, A_2, A_3	μA709	High performance Op-Amp
D_1, D_2, D_3	1S920	Silicon diode
D_4	1S2120	12v zener
P_1	5 kΩ	Pre-set
R_{A1} to R_{A4}	1 kΩ	0.1 % precision W.W.
R_{B1}	1 MΩ	5% Hystab
R_{B2}	330 kΩ	5% Hystab
R_{B3}	220 kΩ	5% Hystab
R_{B4}	150 kΩ	5% Hystab
R_5, R_8, R_{11}, R_{14}	15 kΩ	5% Hystab
R_6, R_9, R_{12}, R_{15}	1.5 kΩ	5% Hystab
R_7, R_{10}, R_{13}, R_{16}	430 Ω	5% Hystab
S_1 to S_8	HRC1 (RTS)	Mercury reed. Coils operate at 2V, 100 mA
T_1, T_6 to T_9	C426	NPN medium power
T_2 to T_5	2N3704	NPN with low $V_{CE(SAT)}$

Table 5.1 Components table for fig. 5.1

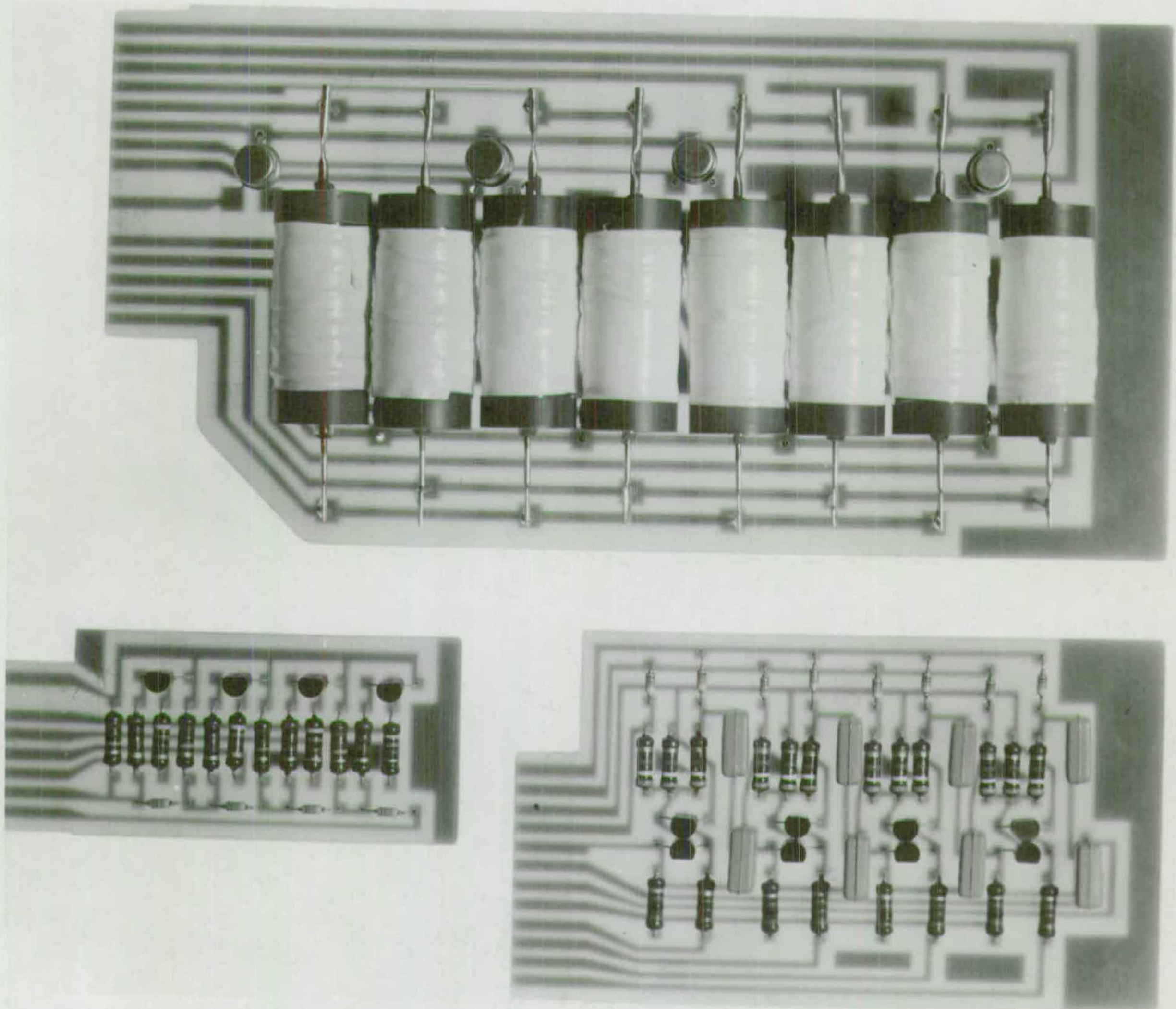

Figure 5.2 Printed circuit cards for D-to-A generator

at terminal A, and the correction signal is derived from the currents through R_{B1} to R_{B4}, summed at terminal B. A and B are maintained near earth potential by the operational amplifiers A_1 and A_2. When the first stage is switched in, S_1 conducts, S_2 to S_7 are open, and the currents through R_{A1} and R_{B1} are modulated by the ladder output via amplifier A_3 and transistor T_2. The biasing of T_2 to T_5 is such that only T_2 conducts at this stage. When the ring counter switches to the second stage (T_7 conducting), S_2 clamps R_{A1} and R_{B1} across the ladder reference voltage and the feedback to A_3 is now switched by S_3 to R_{A2} and R_{B2}. T_3 conducts, and T_4 and T_5 are still biased off. R_7 is chosen to allow T_2 to be near saturation at switchover so the current through S_2 is minimised, similarly for the remaining two stages. The resistors R_{B1} to R_{B4} may be replaced by suitable non-linear elements built up from zener diodes and resistors. These resistors are chosen so that the current at terminal B increases in four linear segments giving a signal which is approximately proportional to the square of the current through A.

The differential amplifiers have offset voltages of less than 1mV which is less than a 1-bit increment in the ladder output, so the output accurately expands the input dynamic range by a factor of four. The linearity of this output is, however, limited by the tolerance of the precision resistors.

Mercury reed switches, actuated by low impedance coils, were chosen in order to simplify the design and construction of the prototype and ensure accuracy. Their main drawbacks are their bulk and slow response time, but these hardly matter in the present application. The slow response gives rise to transients in the output of up to 2mS duration, so the EBM is programmed to cut off the beam for this period at each switchover. By using MOS FET's to switch in the feedback, and transistors switching in the reference source, the transients can be reduced and a much higher input rate allowed.

Most of the components for four stages of the circuit are mounted on three printed circuit cards (figure 5.2). It is thus convenient to assemble a system with 8, 12, or 16 stages, etc., using these boards. The design makes use of several integrated circuit modules. These include the operational amplifiers and the components of the primary D-to-A voltage source. For the prototype, a discrete component version of the reversible ring counter was built, but again this may well be replaced by an integrated circuit version. The design of the power supply is important. In particular a very high order of stability is demanded from the reference supply, and to achieve this special voltage reference diodes are available (e.g. the Motorola MZ605 - long term stability <5ppm./1000hrs. and temperature drift 5ppm./^{o}C). Because of the high rejection ratio of the operational amplifiers the drift in the

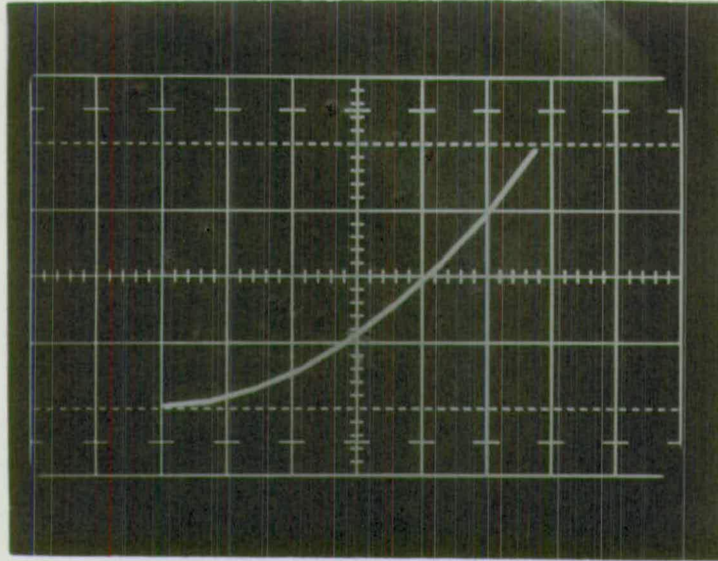

Figure 5.3 Correction signal v. linear output

main supply is not so critical. Ripple should be reduced to 1ppm. in the main supply using a circuit similar to that of figure 3.8.

Figure 5.3 shows the response from the prototype, which is in fact a single channel eight stage version. By increasing the number of stages still futher, a dynamic range of up to 100,000 is feasible. However the long term repeatability, determined mainly by drift in the resistors and reference supply, would not normally approach this figure. It should be noted, that for EBM applications a very large dynamic range and adequate short term repeatability are important features, but a high degree of linearity in the output is not necessary.

If it is possible to increase the dynamic range to 100,000, then this would represent a total of 10^{10} cô-ordinates in the XY plane. The input register should then be programmed with at least 10^{7} bits per second in order to reduce the machining time to below 1000 seconds. The maximum rate between reversals of counting direction for the register, would however be limited by the frequency response of the deflection coils. This would typically be about 100kc/s.

5.2 PANTOGRAPH CONTROLLER

The circuit of a pantograph control system is shown in figure 5.4.

It is planned to use this system as an auxiliary method of programing and controlling the beam deflection. The advantages of this system, which have already been discussed in chapter 1, are that it is a ready method for immediately transposing design ideas to the EBM, and also it is a very simple and inexpensive stand-by system.

The complete system is conveniently separated into four stages, the first stage comprising the electro-mechanical transducers. By means of the linear potentiometers P_1 and P_2, the instantaneous position of the tracing pen (see figure 1.2(b)) is converted to two voltage signals. The high sensitivity and stability of the operational amplifiers A_1 and A_2 means that the potentials across P_1 and P_2 need only be of the order of 100mV, so rather than using expensive wirewound or film potentiometers, P_1 and P_2 can be of simple slide-wire construction. The capacitors C_1 and C_2 perform the function of velocity transducers. Their common connection at S_1 is virtually at a fixed potential, so the currents in C_1 and C_2 are accurately proportional to the rate of change of voltage across the potentiometers.

The second stage is a twin voltage to current amplifier which feeds the X and Y deflection coils. The amplifiers A_1 and A_2 have integrated circuit inputs feeding power transistor emitter-follower output stages. The voltage to current gain ratio is

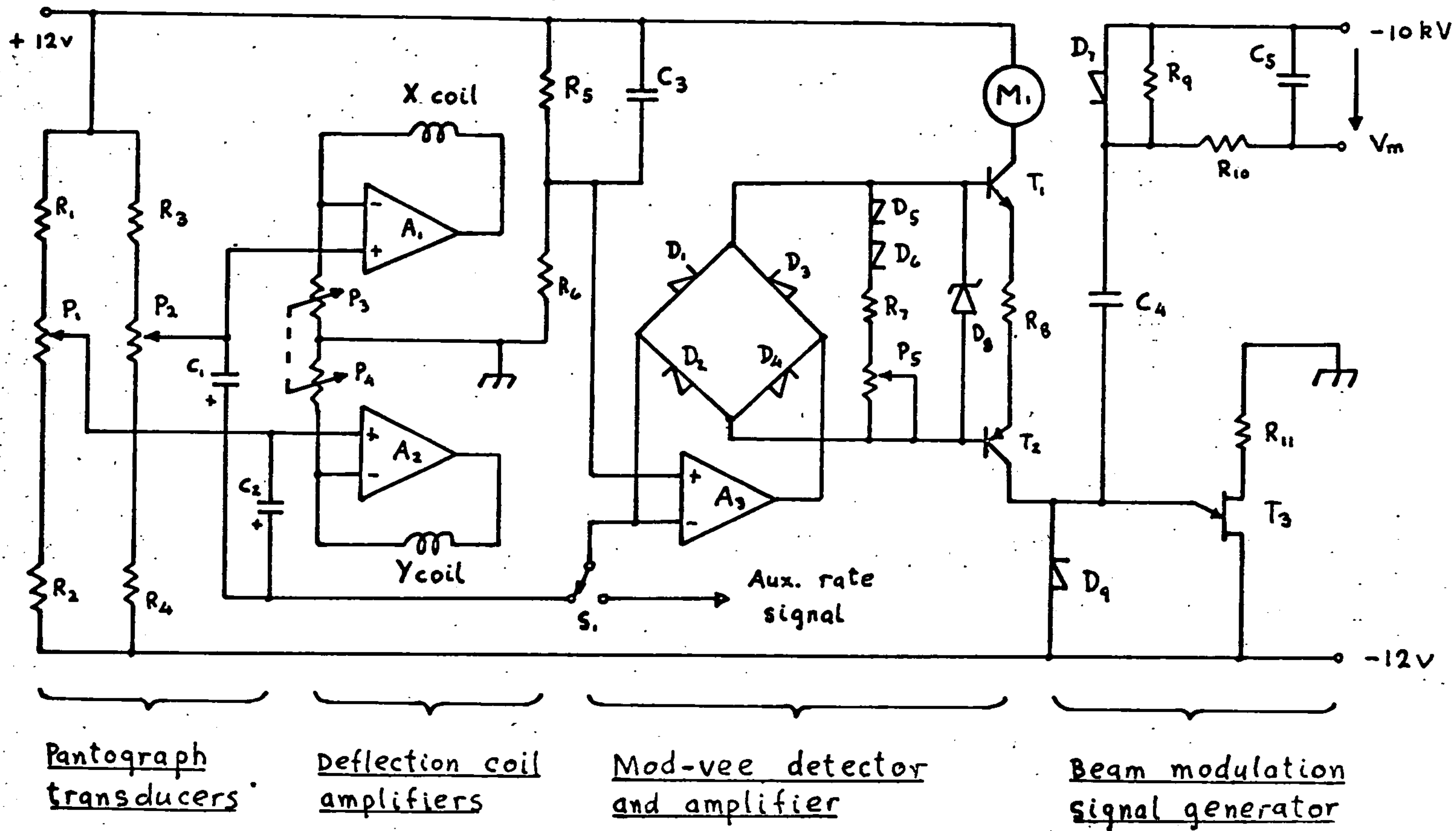

Figure 5.4 Circuit for the pantograph controller

varied by P_3, P_4, and covers a range of outputs from a few milliamps to about one amp maximum.

The "mod-vee" detector and amplifier stage measures the current at S_1, rectifies or polarises this signal, and amplifies it to a suitable level to drive the final stage. The inputs of A_3 are at +6 volts in order to bias the electrolytic capacitors C_1 and C_2, and also to bias the voltage level of the output to T_3. By using a bridge rectifier in the feedback loop to the inverting input (of A_3), the voltage impressed across the feedback resistor network R_7 and P_5 is always positive, and this voltage is proportional to the current through S_1. The transistors T_1 and T_2 form a voltage to current amplifier with floating differential inputs. D_5 and D_6 compensate for the base-emitter voltages of T_1 and T_2, and the zener diode D_8 determines the maximum current output. The meter M_1 is calibrated in percentage of this maximum current.

Since the capacitor currents are summed algebraicaly at S_1, this method of velocity measurement is only accurate if movements in the X and Y directions are made sequentially and not simultaneously. If this is a restriction, an electro-mechanical transducer which measures the magnitude of any velocity vector may be employed as an auxiliary signal, but to achieve this with the required accuracy would be quite complex. A ready but again

expensive alternative is to use analog computing elements to perform the function $(a^2 + b^2)^{\frac{1}{2}}$.

The final stage is a beam-modulation signal generator which takes a signal from the mod-vee stage and matches the beam current with the writing speed of the pantograph operator. In this way the charge per unit length of scan on the workpiece is held constant, and machining quality is kept uniform for a fairly wide range of writing speeds. In particular when the pen is stationary the beam current must be adjusted to zero. The operation of this final stage is similar in principle to the beam-modulation circuit described in section 3.5.

5.3 DEFLECTION COIL DESIGN

The aberrations of the focussed spot which occur with beam deflection and which were discussed in section 2.7, fall into two categories - those due to astigmatic de-focussing, and chromatic aberration due to the energy spread in the beam electrons. The former can be reduced by carefully designing the deflection coils or by superimposing suitable correction fields, in addition to dynamic focussing. This type of error increases rapidly with deflection angle and width of beam, so it is a great advantage to use a relatively long working distance and a very small final aperture. This is quite possible with a very high brightness

source such as the field emission source, provided the design of the final lens is suitable for long focal lengths.

Chromatic error is less easy to reduce by conventional methods since the error occurs for paraxial and marginal rays equally, and since the error is invariable for any given dynamic range irrespective of deflection angle or working distance. The effect of this aberration is not usually encountered, but for the present case where a dynamic range of up to 100,000 is aimed for, the error becomes apparent at beam potentials below 10kV. (This is based on the calculation of equation (2.20), and assumes an energy distribution half-width of 0.1eV for electrons emitted from a field emission source). Short of including some means of energy filter, which apart from its inconvenience would probably add further aberration, this appears to be the limiting factor for the best resolution.

Various approaches to the design of high performance deflection optics have been tried. Schlesinger and Wagner[17] have described a system which in addition to having dynamic focus control uses an octupole stigmator to dynamically correct astigmatism. This is a powerful method for reducing deflection aberrations, and results showed that a dynamic range of 9000 in both X and Y direction was achieved with their apparatus. This figure is relative and one could expect an even greater range if improvements

in beam geometry were made. An important part of their system was a specially developed signal generator which was used to drive the octupole and adjust the focus. This could generate the quadratic terms for the octupole (see figure 2.4) which include an X.Y product. The D-to-A controller described in section 5.1 does not generate X.Y product terms, so it could not provide astigmatism compensation in its present form but would require in addition an electronic product generator.

An alternative method of controlling astigmatism is to optimise the field distribution of the deflection coil. This has been done by Wang[15] using a computer program to calculate the aberrations. For the case of one-dimensional deflection and for a given beam geometry he derives the optimum field distribution, and calculates that a dynamic range of about 300,000 is possible with beams of small angular convergence (0.003 radians). However his calculations assume a beam with mono-energetic electrons. His idealised field for one-dimensional deflection is not readily adapted to the two-dimensional case[16].

The coil adopted for the experimental EBM system follows a conventional yoke design. This will be sufficient in the first instance to evaluate the beam spot diameter, and make preliminary adjustments to the dynamic focus signal strength at various focal lengths. An experimental procedure to adjust the field for

minimum astigmatism can be tried later using balanced feeding of two coils, one producing a uniform field and the second having a severe "pin-cushion" field which increases fairly rapidly away from the axis. The optimum pin-cushion field (see section 2.7) can be selected by adjusting the ratio of the currents fed to each coil. Looking at figure 2.3(a) it seems unlikely that the optimum field distribution is in fact symmetrical (about the Z-axis), which suggests that balanced feeding of asymmetrical wedge shaped fields may also be worth investigating.

It appears to be impossible to obtain a field that will deflect a wide cone of electron rays without defocussing. Certainly the best cure for deflection aberration, is to use a very narrow beam that is nevertheless compatible with the required spot intensity.

A final consideration is the frequency response of the deflection coils. This was measured by energising the deflection coil with a constant rms. current sinusoid (150mA), varying from 1 to 200kc/s, and monitoring the voltage induced in a small probe coil set in the centre of the deflection coil field. The deflection coil was supported first on a cardboard former, and secondly on a $1\frac{1}{2}$" stainless steel tube similar to that with which the UHV system is constructed. Using constant current primary excitation the probe voltage should increase linearly with frequency. The results

	Excitation Frequency						
	1	3·3	10	33	100	200	kc/s.
Air	6·6	20	66	180	450	600	mV.
Stainless steel	6·6	20	53	90	80	49	mV.

Table 5.3 Deflection coil probe voltages

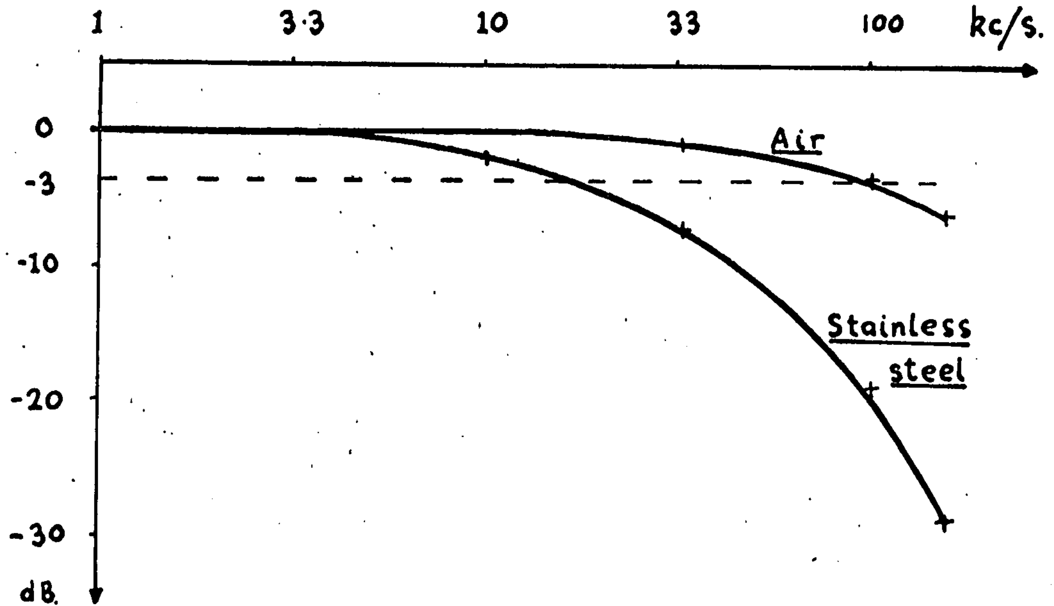

Figure 5.5 Deflection coil frequency response

show that with the coil free-standing in air (cardboard former) the response is 3dB down at 100kc/s, whereas with stainless steel sheilding the response falls 3dB at about 20kc/s (figure 5.5). It was also found that brass and aluminium had very severe damping effect compared to stainless steel.

The present arrangement, with the deflection coils wound outside the column, reduces the practical machining speed considerably. An appropriate solution is to replace the metal column by one of pyrex or ceramic, as this increases the effective bandwidth of the deflection coils and also the solenoid lens. The lens must of course have a high bandwidth for correct dynamic focussing. In addition to this, the effective bandwidth can be extended by introducing high frequency boost in the deflection signal generator, and/or programmed high frequency compensation in the computer output.

CHAPTER 6

REVIEW

The EBM will realise its full potential when a highly automated system capable of reliably machining sub-micron detail is developed. A study has been made of the several parts of the EBM, using an experimental system to test some probable answers to this design problem.

The use of a field emitter gun in the experimental system is an exceptional departure from orthodox design. It is only recently that field emitters have been accepted as having practical engineering applications. This is due to the development of modern UHV systems as well as research into new field emitter materials. With crystal oriented emitters, a new approach to design of the electron-optics can be made. The high brightness allows the use of very small apertures, where diffraction is the limiting aberration rather than spherical aberration, and this factor has boosted the application of field emitters to practical systems.

Recent work by Windsor[32] suggests that crystal oriented lanthanum hexaboride (LaB_6) will eventually replace tungsten as the emitter

material. LaB_6 is a hard refractory material, resistant to ion bombardment. It requires lower applied voltage to induce emission, since it has a very low surface work function of 2.7eV. Thus the energy of bombarding ions is lower and this can result in a lower rate of tip erosion. However the material is difficult to machine and requires special etching techniques.

An experimental method which allows field emitters to operate at conventional vacuums has been described in chapter 3. This opens the way to "low grade" performance of field emitters, which nevertheless may prove superior to conventional cathode performance, and at the same time is competitive in cost and simplicity. The behaviour of "low grade" field emitters should be studied in detail in a system with close control of the pressure and residual gas composition, and preferably with a scanning electron microscope facility in the same vacuum chamber to monitor detail of the tip geometry.

To limit the cost and simplify experimental procedure, the UHV system has remained of simple design, using only five or six basic components. Some idea as to what should be the final form for an operational EBM have been worked out. A differential pumping system between gun and work chamber would allow the chamber to be cycled from 10^{-6}Torr to atmosphere, while keeping the gun under constant UHV. In a high vacuum system at room temperature, a pressure

difference factor of 10^3 across an aperture of 0.1mm. results in a leakage of only 1 litre/second into the lower pressure side[33]. This leakage can be pumped away by a small 10 litre/second ion pump, and the aperture may serve a dual purpose by creating the pressure difference and also forming the defining aperture for the electron beam. In addition, a straight through plate valve should be included to isolate the work chamber when cycling down to atmosphere.

The option of making the column in pyrex or ceramic has been mentioned in section 5.3. This would greatly increase the bandwidth of the deflection and focussing coils, if these were wound outside the column. An extra benefit is the possibility of using RF heating to outgass the metal electrodes inside the column, using an external induction coil.

A great deal of effort was put to designing the electronic instrumentation. This is of course an integral part of the EBM system and should be "tailor made" for the application. The D-to-A generator forms the central part of the computer-to-EBM interface, while facilities for computer control were also built into the high voltage current source. In the near future, a master voltage reference source with ultra low drift will be installed, and will control all the power supplies for the deflection generator, lens supply, high voltage source, and any additional instrumentation

used in the EBM system.

These developments will eventually lead to a highly controlled precision machine, with an important contribution in the realm of micro-miniature, high reliability devices.

REFERENCES

1. Millard, P.A. — Microelectronics and Reliability, 4, 1965, 25-

2. Thornley, R.F.M. & Hatzakis, M. — Record IEEE 9th Annual Symposium on Electron, Ion, and Laser Beam Technology, BERKLEY 1967, 94-

3. Chang, T.H.P. & Nixon, W.C. — ibid., 123-

4. Oatley, C.W. et al. — Advances in Electronics and Electron Physics, 21, 1965, 181-

5. Legg, C.R.E. — Microelectronics and Reliability, 4, 1965, 31-

6. Pierce, J.R. — Theory and Design of Electron Beams, VAN NOSTRAND, 1954, 76-

7. Glaser, W. — Zeit. Physik, 118, 1941(b), 264-

8. Grivet, P. — Electron Optics, PERGAMON, 1965, 35-

9. Okoshi, T. — IEEE Trans. on Electron Devices, 12, 1965, 564-

10. Liebmann, G. — Proc. Physical Society, 64B, 1951, 972-

11. Grivet, P. — Electron Optics, PERGAMON, 1965, 424-

12. Langmuir, D.B. — Proc. Inst. Radio Engineers, 25, 1937, 977-

13. Young, R.D. & Muller, E.W. — Physical Review, 113, 1959, 115-

14. Everhart, T.E. — Record IEEE 9th Annual Symposium on Electron, Ion, and Laser Beam Technology, BERKLEY 1967, 15-

15. Wang, C.C.T. — IEEE Trans. on Electron Devices, 15, 1968, 17-

16. Wang, C.C.T. — ibid., 15, 1968, 603-

17. Schlesinger, K. & Wagner, R.A. — IEEE Trans. on Electron Devices, 12, 1965, 478-

18. Schurmann, J. & Haussmann, G. — Zeit. angew. Physik, 22, 1967, 235-

19. Grivet, P. — Electron Optics, PERGAMON, 1965, 233-

20. Broers, A.N. — Record IEEE 9th Annual Symposium on Electron, Ion, and Laser Beam Technology, BERKLEY 1967, 1-

21. Martin, E.E. *et al.* — Jnl. Applied Physics, 31, 1960, 782-

22. Everhart, T.E. — First Int. Conf. on Electron and Ion Beam Science and Technology, WILEY, 1965, 341-

23. King, H.N.G. — Microelectronics, 1, 1967, 28-

24. Ramey, R.L. — Physical Electronics, PRENTICE-HALL, 1961, 101-

25. Crewe, A.V. *et al.* — Rev. Scientific Instruments, 39, 1968, 576-

26. Dolan, W.W. & Dyke, W.P. — Physical Review, 95, 1954, 327-

27. Crewe, A.V. *et al.* — Rev. Scientific Instruments, 40, 1969, 241-

28. Dyke, W.P. *et al.* — Jnl. Applied Physics, 31, 1960, 790-

29. Bloomer, R.N. — Brit. Jnl. Applied Physics, 8, 1957, 83-

30. Dyke, W.P. & Dolan, W.W. — Advances in Electronics and Electron Physics, 8, 1956, 89-

31. Klemperer, O. — Electron Physics, BUTTERWORTHS, 1959, 41-

32. Windsor, E.E. — Proceedings IEE, 116, 1969, 348-

33. Guthrie, A. — Vacuum Technology, WILEY, 1963, 510.

ACKNOWLEDGEMENTS

I am indebted to Professor W.E.J. Farvis and Dr. A.R. Dinnis for their guidance throughout this work.

I would like to thank the Science Research Council for their financial support during the entire period of study.